Chemical Composition-Dependent Hygroscopic Behavior of Individual Ambient Aerosol Particles Collected at a Coastal Site

Li Wu[1,2,+], Hyo-Jin Eom[1,3,+], Hanjin Yoo[1,4], Dhrubajyoti Gupta[1], Hye-Rin Cho[1], Pingqing Fu[2], and Chul-Un Ro[1,4,*]

[1] Department of Chemistry, Inha University, Incheon 22212, Korea
[2] Institute of Surface-Earth System Science, School of Earth System Science, Tianjin University, Tianjin 300072, China
[3] Air Quality Research Division, National Institute of Environmental Research, Incheon 22689, Korea
[4] Particle Pollution Management Center, Inha University, Incheon 21999, Korea

[*] ***Correspondence to*** Chul-Un Ro (curo@inha.ac.kr)
[+]Authors with equal contributions

Abstract

This study investigated the hygroscopic behavior of individual ambient aerosol particles collected at a coastal site of Jeju Island, Korea. The particles' size change along with phase transitions during humidification and dehydration processes, and their chemical compositions, were determined by optical microscopy and scanning electron microscopy-energy dispersive X-ray spectroscopy (SEM-EDX), respectively. Of the 39 particles analyzed, 24 were aged sea-spray aerosols (SSAs) with diverse mixing ratios of Cl^- and NO_3^-.

The ambient SSAs exhibited multiple deliquescence and efflorescence transitions that were dominantly influenced by NaCl, $NaNO_3$, $MgCl_2$, $Mg(NO_3)_2$ and organic species covering the surface of the aged SSAs. For Cl-rich SSAs with $X_{(Na, Mg)Cl} > 0.4$, although some particles showed very slow water uptake at low RHs = ~30%, two major transitions were observed during the humidification process, firstly at RH = ~63.8%, regardless of their chemical compositions, which is the mutual deliquescence relative humidity (MDRH), and secondly at RH = 67.5–73.5%, depending on their chemical compositions, which are the final DRHs. During the dehydration process, the Cl-rich SSAs showed single-stage efflorescence at RH = 33.0–50.5%, due to simultaneous heterogeneous

crystallization of inorganic salts. For Cl-depleted SSAs with $X_{(Na, Mg)Cl} < 0.4$, two prompt deliquescence transitions were observed during the humidification process, firstly at MDRH = 63.8 % and secondly at RH = 65.4–72.9%. The mutual deliquescence transition was more distinguishable for Cl-depleted SSAs. During the dehydration process, step-wise transitions were observed at efflorescence RHs (ERHs) = 24.6–46.0% and 17.9–30.5%, depending on their chemical compositions.

Additionally, aged mineral particles showed partial or complete phase changes with varying RH due to the presence of SSAs and/or NO_3^- species. In contrast, non-reacted mineral and Fe-rich particles maintained their size during the entire hygroscopic process. The mixture particles of organic and ammonium sulfate (AS) exhibited lower deliquescence and efflorescence RHs compared to pure AS salt, highlighting the impact of organic species on the hygroscopic behavior of AS. These findings emphasize the complexity of atmospheric aerosols and the importance of considering their composition and mixing state when modeling their hygroscopic behavior and subsequent atmospheric impacts.

1 Introduction

Atmospheric aerosols play a significant role in the global climate by directly scattering or absorbing incoming solar radiation and indirectly serving as cloud condensation nuclei (Haywood and Boucher, 2000; Pandis et al., 1995). The hygroscopicity of ambient aerosol particles, critically depending on their compositions, is of vital importance in understanding their properties, including their effects on aerodynamic performance, cloud-droplet nucleation efficiency, optical properties, and heterogeneous chemical reactivity with atmospheric gas-phase species (Krueger et al., 2003; ten Brink, 1998; Wang and Martin, 2007; Wu et al., 2020). However, the study of their hygroscopic behavior is challenging because ambient aerosols typically exist as complex mixtures of several chemical species, even at the individual particle level, due to multiphase interactions (Krieger et al., 2012; Pöschl and Shiraiwa, 2015; Schiffer et al., 2018).

Sea-spray aerosols (SSAs) are a significant component comprising 25-60% of atmospheric particulate matter mass (Finlayson-Pitts and Pitts, 2000; Song et al., 2022). Understanding the hygroscopic properties of SSAs is essential for study on aerosol-cloud interactions and global climate (Schill et al., 2015; Zieger et al., 2017), which however, is still defective owing to their complex chemical compositions (Cochran et al., 2017; Meskhidze et al., 2013; Xu et al., 2020). Nascent SSAs are formed when bubbles burst at the sea surface, generating both submicron and supermicron SSAs from film and/or jet drops (Quinn et al., 2015; Wang et al., 2017). The primary inorganic constituents

of nascent SSAs are Na^+, Cl^-, and Mg^{2+}, followed by SO_4^{2-}, Ca^{2+}, K^+, and other minor compositions (Seinfeld and Pandis, 2006). Submicron nascent SSAs contain more organic species and fewer inorganic salts than supermicron ones (Ault et al., 2013; Prather et al., 2013; Wang et al., 2015). In pristine marine environments, the organics in SSAs mostly originate from phytoplankton activities in the sea, while in polluted marine environments, non-biodegradable surfactants from anthropogenic waste run-offs to the sea are supposed to be added (Cochran et al., 2016; Forestieri et al., 2016). Reactions of SSAs with various atmospheric species, such as NO_x/HNO_3, SO_2/H_2SO_4, and CH_3SO_3H, within minutes to hours of residence in air further increase the complexity of the chemical compositions (Liu et al., 2007; Saul et al., 2006; ten Brink, 1998), leading to partially or fully reacted (or aged) SSAs after Cl depletion (Ault et al., 2014; Gard et al., 1998; Laskin et al., 2012; Pósfai et al., 1995; Wu et al., 2020). The further reactive uptake of N_2O_5 was also reported to be dependent on the chloride to nitrate ratio of the reacted SSAs and their phases (Ryder et al., 2014). In addition, SSAs interact with volatile organic carbons (VOCs), secondary organic aerosols (SOAs), etc., in the marine boundary layer (Su et al., 2022). The presence of primary and secondary organics, biogenic species, sea-salt sulfates (ss-SO_4^{2-}), non-sea-salt sulfates (nss-SO_4^{2-}), etc., adds greater complexity to the interdependence of hygroscopic behavior and heterogeneous reactions in ambient SSAs (Ault et al., 2013; Beardsley et al., 2013; Keene et al., 2007; O'dowd and De Leeuw, 2007; Prather et al., 2013).

Many studies have investigated the hygroscopic behavior of both airborne and laboratory-generated SSAs. It is generally accepted that sea-salt-containing particles result in higher hygroscopic factors in supermicron particles (Atkinson et al., 2015; Herich et al., 2009). Some single particle measurements have been reported on ambient fine and coarse mode SSAs that are dominated by inorganic salt species. For example, environmental transmission electron microscopy was used to measure the deliquescence and efflorescence relative humidities (DRHs and ERHs) of NaCl-bearing aerosols, sulfate/chloride containing SSAs, Mg-rich particles, etc., collected from clean and polluted environments (Semeniuk et al., 2007; Wise et al., 2007). It was found that NaCl moiety in sulfate/chloride containing SSAs underwent deliquescence at ~75% RH with the sulfate-bearing phases remaining insoluble, which is similar to the DRH of pure NaCl aerosols, whereas the DRH of the NaCl moiety was lowered in the presence of soluble compositions like $NaNO_3$. In a follow-up study, the DRHs and ERHs of laboratory-generated and ambient SSA particles were found to be consistent (Wise et al., 2009). Similar observations for marine aerosols with insoluble sulfate moieties and a highly hygroscopic NaCl-moiety were also reported (Freney et al., 2010). In-situ Raman spectrometry was

used to probe the phase transitions of SSA droplets (80–100 μm) nebulized from sea-water, which revealed that $CaSO_4 \cdot 0.5H_2O$ solidified at RH > 90%, followed by crystallizations of NaCl and $KMgCl_3 \cdot 6H_2O$ at RH = ~55% and ~44%, respectively (Xiao et al., 2008). Optical microscopy combined with low-*Z* particle energy-dispersive electron probe X-ray microanalysis (low-*Z* particle EPMA) was used to determine 2-D growth factors, phase transition RHs, and chemical compositions in ambient aerosols, including nascent and reacted/aged SSAs (Ahn et al., 2010). However, the relationship between hygroscopic properties and the evolving chemical compositions and mixing states of ambient SSAs remains unclear.

Laboratory-generated inorganic salt particles have been utilized as surrogates to understand and parameterize the complex hygroscopic properties of SSAs for climate models. Since NaCl constitutes approximately 80% of nascent SSAs by mass, the hygroscopic behavior of pure NaCl particles has been extensively studied for parameterizing the thermodynamic and optical properties and cloud activation efficiency of ambient SSAs (Niedermeier et al., 2008; Tang et al., 1997). However, the hygroscopic growth factors of ambient or laboratory-generated SSAs are reported to be different from those of pure NaCl, possibly due to the presence of hydrates such as $MgCl_2 \cdot 6H_2O$, organic substances, or other impurities (Ahn et al., 2010; Guo et al., 2019; Kong et al., 2018; Rosati et al., 2021; Schindelholz et al., 2014; Zieger et al., 2017). Consequently, the hygroscopic properties of multicomponent systems such as mixed cation chlorides (Chan et al., 2000; Ge et al., 1996, 1998; Gupta et al., 2015a; Li et al., 2014), sodium salts of mixed anions (Chan et al., 1997; Chang and Lee, 2002; Freney et al., 2010; Gupta et al., 2015b), and other mixture systems such as NaCl-$MgSO_4$ (Woods et al., 2010), NaCl-$CaSO_4$ (Freney et al., 2010), NaCl-$(NH_4)_2SO_4$ (Tobon et al., 2021) are of special relevance, which can serve as surrogates for ambient or reacted SSAs.

As discussed in detail elsewhere (Gupta et al., 2015a; Li et al., 2014), thermodynamic principles predict stepwise phase transitions in two-component inorganic solid salt mixtures, such as NaCl-KCl, NaCl-$MgCl_2$, and NaCl-$NaNO_3$, that can dissolve during the humidification process (Wexler and Seinfeld, 1991). When the mixing ratio of the two-component is at a certain value, e.g. $X_{NaCl} = 0.38$ (or $X_{NaNO_3} = 0.62$) in the NaCl-$NaNO_3$ mixture, particles act like a single-salt and exhibit a single phase transition at its mutual DRH (MDRH), where the mixture is considered to have a eutonic composition. For particles with other mixing ratios, the first transition generally occurs at their MDRH, regardless of the specific ratios; and the resulting aqueous phase from partial deliquescence also possesses the eutonic composition. As RH further increases, partially dissolved particles continue to absorb water

until the remaining solid component fully dissolves at the respective DRH, dependent on the salt moiety richer in concentration. During the dehydration process, as RH decreases, the concentration of the richer salt moiety becomes more concentrated, leading to crystallization at their respective ERH. The aqueous phase of the eutonic composition then effloresces at their mutual ERH (MERH) as RH further decreases.

Thermodynamic models, such as the Extended Atmospheric Inorganics Model (E-AIM) (http://www.aim.env.uea.ac.uk/aim/aim.php; (Ansari and Pandis, 1999; Carslaw et al., 1995; Clegg et al., 1998b, a; Wexler and Clegg, 2002) and the Aerosol Inorganic-Organic Mixtures Functional groups Activity Coefficients (AIOMFAC) (http://www.aiomfac.caltech.edu; Zuend et al., 2008, 2011), can predict MDRHs and DRHs for multicomponent mixture systems. The DRH represents the solubility limit (saturation concentration) of a compound in a solution, defining solid–liquid equilibrium. When a solid compound coexists with a saturated liquid mixture, it has a specific molar ion activity product (IAP) in that solution. The AIOMFAC model calculates IAP as a function of RH using ion activity coefficients, which remains constant regardless of other mixture components. The corresponding RH becomes the DRH when the calculated IAP matches that of saturated solutions. However, as efflorescence is a kinetic or rate-driven process, no general theoretical model can predict the efflorescence of single or multicomponent aerosol particles, and thus the best way is experimental observation (Cohen et al., 1987; Martin et al., 2000). Previous modeling and field studies have attributed the reduction in hygroscopic growth of SSAs to the organic fractions (Ming and Russell, 2001; Vaishya et al., 2013; Zhang et al., 2014), whereas recent measurements suggest that organic species have an insignificant influence (Nguyen et al., 2017). Therefore, establishing a systematic correlation between the chemical compositions and hygroscopic behavior of ambient SSAs vis-à-vis the multicomponent inorganic surrogates is a priority towards understanding the hygroscopic properties of ambient SSAs and parametrizing phase changes for model applications.

Mineral particles, such as aluminosilicates and calcium carbonate, which are typically non-hygroscopic, can become hygroscopic when they are internally mixed with SSAs or react with gaseous species such as NO_x, SO_2, and organic acids in the presence of water vapor (Li et al., 2014; Tang et al., 2016). In fact, mineral dust and aged SSAs may exist as internal and/or external mixtures in the atmosphere (Geng et al., 2014). For instance, Mg-silicate particle coagulated with SSA partially increased in size only at the SSA region with increasing RH and was covered with an aqueous droplet caused by the complete dissolution of the SSA part in high RH (Semeniuk et al., 2007). Additionally,

aluminosilicates coated with sulfur-bearing materials or internally mixed with sea salt particles can absorb water, although the aluminosilicates remained as solid phases (Freney et al., 2010).

In this study, we systematically investigated the hygroscopic behavior of ambient aerosols collected on Jeju Island, Korea, together with their chemical compositions in various mixing states on a single particle basis. Especially, the hygroscopic properties and chemical compositions of ambient SSAs were examined and compared with multicomponent inorganic surrogate systems containing Na^+, Mg^{2+}, Cl^-, and NO_3^-. The phase transitions were observed by monitoring the 2-D size changes of the particles as a function of RH under optical microscopy and the hygroscopic curves and phase diagrams were derived. To determine the chemical compositions of the individual ambient aerosols and the spatial distribution of elements in the effloresced particles, we used scanning electron microscopy/energy dispersive X-ray spectroscopy (SEM/EDX) and analyzed their X-ray spectra and maps, respectively. Although ambient aerosols are complex in their compositions and hygroscopic properties, the detailed elucidation of their hygroscopic behavior according to chemical compositions of ambient aerosols can contribute to the ongoing efforts to improve our understanding of atmospheric aerosols and their impacts on global climate.

2 Experimental Section

2.1 Samples

Ambient aerosol particles

Aerosol samples were collected on April 16 and 17, 2012, at the Gosan meteorological site (33.29°N, 126.16°E) located on the west coast of Jeju Island in South Korea (see Fig. 1). Ambient aerosols were loaded on TEM grids (200-mesh Cu coated with Formvar stabilized with carbon, Ted Pella, Inc.) mounted on stages 2 and 3 of a three-stage cascade PM_{10} impactor (Dekati Ltd.) with aerodynamic cut-off diameters of 10–2.5 μm and 2.5–1.0 μm, respectively, at a flow rate of 10 L min^{-1}. Sampling durations for each stage were adjusted to collect an appropriate number of particles without overloading. The samples were put into black plastic boxes and sealed with parafilm immediately after the collection and these sealed samples were then stored in a refrigerator before the measurements. Stage 2 particles, which were sized between 10-2.5 μm, were used to measure chemical composition and hygroscopic behavior in this study.

Laboratory-generated (Na, Mg)(Cl, NO_3) mixture particles

In the previous studies (Gupta et al., 2015a, b; Zhang et al., 2004), aerosols of NaCl, $NaNO_3$, $Mg(NO_3)_2$, NaCl-$NaNO_3$, and NaCl-$MgCl_2$ were extensively investigated. As Na^+, Mg^{2+}, Cl^-, and NO_3^- are major species of the ambient SSAs collected in our samples, based on low-*Z* particle EPMA results, we measured the hygroscopic behavior of NaCl-$MgCl_2$-$NaNO_3$-$Mg(NO_3)_2$ surrogate system in this work to simulate ambient SSAs that contain similar major elements. Pure solutions (1.0 M each) of NaCl (>99.9% purity, Aldrich), $MgCl_2 \cdot 6H_2O$, and $NaNO_3$ (99.9% purity, Aldrich) were prepared using de-ionized water (18 MΩ, Millipore Direct-QTM). The pure solutions were then mixed to obtain solutions with $[Cl^-]$:$[NO_3^-]$ = 3:1, 1:1, and 1:3 (i.e. $X_{(Na,Mg)Cl}$ = 0.75, 0.5, and 0.25), while maintaining the sea water ratio of $[Na^+]$: $[Mg^{2+}]$ = 9:1 (Haynes, 2015), as the elemental ratio of Na and Mg in the ambient SSAs from our samples is also approximately 9. A single jet atomizer (HCT4810) was used to generate aerosol particles from the mixture solutions on hydrophobic TEM grids. Herein, a notation system is used to represent aerosol particles of NaCl-$MgCl_2$-$NaNO_3$-$Mg(NO_3)_2$ as (Na, Mg)(Cl, NO_3).

2.2 Hygroscopic property measurements

The experimental setup for measuring hygroscopic behavior consists of three main components: (A) a see-through impactor, (B) an optical microscope, and (C) a humidity control system. The TEM grid with aerosol particles was attached to the impaction plate in the see-through impactor, and the RH was controlled by mixing dry and wet gaseous N_2 (99.999% purity) flows that were adjusted to obtain the desired RH in the range of ~5.0−92.0%. The humidity control system used wet N_2 gas obtained by bubbling through deionized water reservoirs. The RH was monitored by a digital hygrometer (Testo 645) that was calibrated using a dew-point hygrometer (M2 Plus-RH, GE) to provide RH readings with ±0.5% reproducibility. A detailed discussion of the impactor and humidity-controlling system can be found elsewhere (Li et al., 2021). The particles were continuously imaged in RH = 1% steps using a digital camera (Canon EOS 5D, full frame, Canon EF f/3.5 L macro USM lens) mounted on an optical microscope (Olympus, BX51M) during the humidification process (by increasing RH from ~5.0 to 92.0 %), followed by the dehydration process (by decreasing RH from ~92.0 to 5.0 %). The changes in particle size with the variation of RH were monitored by measuring the particle areas in the optical images to generate hygroscopic curves. Each humidity condition was sustained for at least 2 mins to allow for sufficient time for water condensation or evaporation. The hygroscopic curves are represented by the area ratio (A/A_0) as a function of RH, where the 2-D projected aerosol area at a given RH (A) is divided by that before starting the humidification process (A_0). The images were processed using image

analysis software (Matrox, Inspector v9.0). The experiments were conducted at room temperature (T = 22 ± 1 ºC). Pure NaCl particles were used to verify the accuracy of the system with DRH = 75.5 (± 0.5) % and ERH = 46.3–47.6 %.

2.3 Low-*Z* particle EPMA measurements using SEM-EDX

The ambient aerosol particles were analyzed using low-*Z* particle EPMA measurements with a Jeol JSM-6390 SEM equipped with an Oxford Link super atmospheric thin window (SATW) EDX detector. The analysis was conducted both before and after the hygroscopic processes to find out fields on TEM grids with well-separated particles based on their secondary electron images (SEIs, ~ 100 µm x 100 µm for a field) and to determine the morphology, chemical composition, and spatial distribution of the chemical elements (elemental maps), respectively. The resolution of the detector was 133 eV for Mn Kα X-rays. Point mode and area mode X-ray spectra and elemental maps of individual particles were recorded using Oxford INCA Energy software. An accelerating voltage of 10 kV and beam current of 0.5 nA were used, and typical measurement durations were 20 sec. for point mode, 1 min. for area mode, and 5-10 min. for elemental mapping.

The AXIL program was used to obtain the net X-ray intensities for chemical elements through non-linear least-squares fitting of the spectra. From these intensities, the elemental concentrations of individual particles were determined (Vekemans et al., 1994). For individual particles sitting on TEM grids, C and O concentrations were determined using a Monte Carlo calculation technique to correct for the interfering X-ray peaks of C and O emitted from the TEM grid, providing accurate quantification results (Geng et al., 2010). A detailed explanation of the elemental quantification procedure can be found elsewhere (Wu et al., 2019).

3 Results and Discussion

3.1 Chemical composition and hygroscopic behavior of individual ambient aerosol particles

In this study, a total of 39 particles on three fields were investigated, including 24 aged/reacted SSAs with diverse mixing ratios of Cl^- and NO_3^- and 15 other particles such as six aluminosilicates, five Ca-containing particles, two Fe-rich particles, an aged SiO_2, and a mixture particle of organic and $(NH_4)_2SO_4$. The mole fraction of Cl as $X_{(Na,Mg)Cl}$ in the aged/reacted SSAs was calculated based on $[Cl^-]/([Na^+]+2[Mg^{2+}])$ to determine the degree of Cl-depletion in the SSA particles. Fig. 2 shows the SEI of the first field containing 16 particles, where the chemical species of each particle are indicated,

together with two exemplar X-ray spectra of aged SSAs #5 and #11 with $X_{(Na,Mg)Cl}$ = 0.75 and 0.23, respectively. The elemental concentrations of all particles and their chemical species, determined by X-ray spectral analysis, are listed in Table S1 of Supporting Information.

In Fig. 3, optical images obtained at different RHs during the humidification and dehydration processes and the secondary electron image (SEIs) after hygroscopic process for 16 particles on the first field are shown. Except particles #2, #4, #7, #8, and #14, the rest are aged SSAs. Optical images and the SEIs for particles on the second and third fields are provided in Figs. S1 and S2, respectively. Particles were initially solid at RH = 5.3 % before the hygroscopic measurement, as shown in Fig. 3A. During the humidification process, most of the SSAs showed partial deliquescence at RH = 63.8 % (Fig. 3C), regardless of their aging degree, indicating the realization of the MDRH. Upon further increase of RH, SSAs underwent full deliquescence transitions at DRH = 65.4 – 73.5 %, which varied for each SSA, as shown in Figs. 3D and E. During the dehydration process, almost all SSAs exhibited colored ring-type patterns (Figs. 3G and H) due to the diffraction of visible light typically observed in the presence of organic surfactants on water, indicating the presence of considerable amounts of organic species in aged SSAs. SSA droplet #5 crystallized at ERH = 50.5 % (Fig. 3G), while the others effloresced over a lower range of ERH = 46.0 – 17.9%. The various DRHs and ERHs indicate different chemical compositions of SSAs.

Aluminosilicates and Fe-rich particles did not exhibit any water uptake or changes as a function of RH. Aged aluminosilicates, aged SiO_2, and some reacted Ca-containing particles showed modest growth/shrinkage continuously due to the presence of amorphous NO_3^- phases (Ahn et al., 2010). The mixture particle of organic and ammonium sulfate experienced distinct deliquescence and efflorescence. Detailed description of hygroscopic behavior of the ambient aerosol particles is given as follows.

3.2 SSA particles

The average atomic concentrations of C, Na, Cl, N, Mg, S, K, and Ca in SSAs are listed in Table S1 with the values being 43.0(±7.2)%, 13.6(±4.6)%, 8.0(±6.6)%, 7.9(±2.3)%, 1.5(±0.4)%, 0.8(±0.3)%, 0.3(±0.1)%, and 0.3(±0.1)%, respectively. The elemental analysis of the SSAs indicates that they consist primarily of Na^+, Mg^{2+}, Cl^-, NO_3^-, and organic species. The elemental concentration of N is significantly higher than that of S, and the elemental ratio of S and Na in the ambient SSAs collected from our samples closely resembles that of sea water ([S]/[Na] = 0.06; Haynes, 2015). As a result, the SSAs is considered to contain more nitrate due to the rapid reaction with NO_x/HNO_3, as opposed to

sulfate. As the SSAs become more aged or reacted, their mole fractions of Cl^- relative to Na^+ and Mg^{2+} decrease, while their mole fractions of NO_3^- increase. Although the aged/reacted SSAs are a complicated multi-component system as a fraction of ambient aerosols, (Na, Mg)(Cl, NO_3) mixture system is considered as an inorganic surrogate system for understanding their hygroscopic behavior. The AIOMFAC model predicts the eutonic compositions of Na(Cl, NO_3) and (Na, Mg)(Cl, NO_3) mixture systems as X_{NaCl} = 0.38 and $X_{(Na,Mg)Cl}$ = 0.46, respectively. The mole fraction of Cl in the eutonic compositions of the inorganic component of the aged SSAs would be around 0.4. And thus, the SSAs can be classified as Cl-rich or Cl-depleted depending on their $X_{(Na,Mg)Cl}$ values being greater or less than 0.4, respectively.

3.2.1 Cl-rich SSAs

Fig. 4 displays the projected 2-dimensional (2-D) area ratio and optical images for Cl-rich SSAs #5 and #19 (panels a and d, respectively), and the 2-D area ratio of humidification (panels b and e) and dehydration (panels c and f) for the two SSAs as a function of RH. For SSAs #5 and #19 the mole fraction of chloride, $X_{(Na,Mg)Cl}$ was calculated to be 0.75 and 0.72, respectively. In addition, the figure also includes the (Na, Mg)(Cl, NO_3) particle with $X_{(Na,Mg)Cl}$ = 0.75 for comparison.

During the humidification process, SSAs #5 and #19 initially remained constant in size until RH reached around 30%, after which they gradually increased in size. This behavior is also consistent with the (Na, Mg)(Cl, NO_3) system (Figs. 4b and e), suggesting that $MgCl_2 \cdot 6H_2O$ (DRH = 33.3 %) or Mg^{2+}-rich eutonic part may have undergone water absorption (Gupta et al., 2015a; Zieger et al., 2017). However, the deliquescence transitions were not as distinct as those in particles with $X_{(Na,Mg)Cl}$ = 0.25 and 0.5 generated from (Na,Mg)(Cl,NO_3) mixture solutions (see Fig. S3 in the Supporting Information). The size increase was followed by a shrinkage until RH = 60.5% due to structural rearrangement in the remaining undissolved salt-mixture crystals. Structural rearrangements are commonly observed after preliminary absorption of water at RHs just before the prompt deliquescence transition (Ahn et al., 2010; Gupta et al., 2015a,b; Mikhailov et al., 2009). At first DRH = 63.8%, a partial droplet-like shape appeared in the particle morphology although there was no significant change in the 2-D area ratio. Clear final deliquescence transitions were observed in both SSAs #5 and #19 at DRHs = 73.5 % and 72.9 %, respectively, due to the dissolution of the remaining solid NaCl moiety in these Cl-rich particles. The measured DRHs of SSAs #5 and #19 were closer to the final DRHs calculated for the Na(Cl, NO_3) system using the AIOMFAC model (Fig. 6), and higher than the calculated and measured ones in the

(Na, Mg)(Cl, NO_3) particles (Figs. 4b and e and Fig. 6). These observations for the Cl-rich SSAs suggest that most of the Mg^{2+} salts ($MgCl_2 \cdot 6H_2O$ with DRH = 33.3 %; $Mg(NO_3)_2$ with DRH = 52%) have already dissolved at low RHs or undergone complexation with organic moieties (Eom et al., 2016), and the remaining NaCl and $NaNO_3$ moieties drove the deliquescence transition. The hygroscopic growth of both SSAs #5 and #19 was much smaller than that of the (Na, Mg)(Cl, NO_3) system (Figs. 4b and e) when RH was raised to 91.4%, indicating the presence of a partitioning hydrophobic layer composed of organic surfactants that covered the aqueous salt droplets and inhibited water uptake (Bertram et al., 2018; Cochran et al., 2016; Eom et al., 2016; Lee et al., 2020).

During the dehydration process as RH decreased from ~91% to ~5%, both the SSA droplets showed a continuous shrinkage in size before their efflorescence. However, the rate of shrinkage was much smaller than that of pure inorganic surrogates, such as the (Na, Mg)(Cl, NO_3) system with $X_{(Na,Mg)Cl} = 0.75$ (Figs. 4c and f), indicating that the hydrophobic surfactant layers covering the aqueous salt droplets potentially impeded the water evaporation. SSAs #5 and #19 showed one clear efflorescence transition at RH = 50.5% and 45.0%, respectively (Figs. 4a and d). Interestingly, SSA #5 ($X_{(Na,Mg)Cl} = 0.75$) underwent a sharp decrease in size from RH = 50.9 – 50.5%, which is considerably higher than the ERH range of ~45 – 47% for pure NaCl particles (Ahn et al., 2010; Eom et al., 2014; Martin, 2000), and the first ERHs of either Na(Cl, NO_3) (Fig. 7) or (Na, Mg)(Cl, NO_3) (Figs. 4c and 7) systems. On the other hand, SSA #19 ($X_{(Na,Mg)Cl} = 0.72$) first showed a small decrease in size at RH = 63.8 – 60.8%, which is not a typical efflorescence transition, followed by a sharp decrease in size at RH = 45.8 – 45.0%, which is on the lower side of the ERH range for pure NaCl and slightly higher than the first ERHs of Na(Cl, NO_3) and (Na, Mg)(Cl, NO_3) systems (Figs. 4f and 7). The higher ERH at RH = 50.5 % in SSA #5 indicates heterogeneous efflorescence of the NaCl moiety, while the ERH = 45.0% in SSA #19 suggests the homogeneous nucleation of NaCl moiety. Both SSA droplets showed just one decisive efflorescence transition at their ERHs, indicating co-crystallization of most aqueous inorganic salt moieties along with NaCl, pointing towards the likelihood that the SSAs with more complicated chemical compositions than the (Na, Mg)(Cl, NO_3) mixture aerosols contain chemicals which can act as seeds, such as (Na, Ca)SO_4 crystals, for the complete crystallization at the efflorescence transition. These observations are substantiated by the distribution of S and O at the center and edge of the NaCl moiety in the X-ray maps obtained from the effloresced SSA particles #5 and #19, respectively (Fig. S4) (Li et al., 2014; Gupta et al., 2015a). The apparent (not so sharp) decrease in size of SSA #19 at RH = 63.8 – 60.8% could be attributed to: (i) the sudden shrinkage of viscous organic

moieties covering the aqueous salt droplet; or (ii) inhibited or slow water loss, probably due to a kinetic barrier to crystallization from amorphous/gel forming moieties such as $MgSO_4$/$Mg(NO_3)_2$/$(CH_3SO_3)_2$(Mg, Ca) (Liu and Laskin, 2009; Xiao et al., 2008; Zhang et al., 2004; Zhao et al., 2006); or (iii) a phase transition, such as heterogeneous efflorescence, had occurred, but the presence of viscous moieties (organics or Mg^{2+}- organic complex) affected the relative 2-D size decrease on the TEM grid substrate.

3.2.2 Equimolar and Cl-depleted SSAs

Fig. 5 shows the plots of the projected 2-D area ratio and optical images for an equimolar SSA #23 (Fig. 5a) and a Cl-depleted SSA #11 (Fig. 5d), and 2-D area ratio of humidification (panels b and e) and dehydration (panels c and f) for the two SSAs as a function of RH. The calculated mole fractions of chloride, $X_{(Na,\ Mg)Cl}$ for SSAs #23 and #11 are 0.52 and 0.23, respectively. The figure also includes the (Na, Mg)(Cl, NO_3) particles with $X_{(Na,\ Mg)Cl}$ = 0.5 and 0.25 for comparison.

During the humidification process, both SSAs #23 and #11 remained relatively constant until RH = ~50 %, unlike the (Na, Mg)(Cl, NO_3) system, probably due to the decreased concentration of $MgCl_2 \cdot 6H_2O$. The particle size then began to shrink until RH = ~59%. Both SSAs exhibited two distinct deliquescence transitions. Partial deliquescence transitions occurred at RH = ~63.8%, which is the MDRH for the mixture of soluble moieties in the ambient SSAs and was reported for the first time. Both SSAs exhibited two clear deliquescence transitions. The observed and AIOMFAC-calculated MDRHs of the Na(Cl, NO_3) system are ~68%, while the AIOMFAC-calculated second MDRH for the (Na, Mg)(Cl, NO_3) system is 66.5% after the dissolution of $MgCl_2 \cdot 6H_2O$ at the calculated first MDRH of ~34%, as shown in Fig. 6. This indicates that the eutonic component in the ambient SSAs, with a lower MDRH of 63.8%, is composed of NaCl, $NaNO_3$, $Mg(NO_3)_2$, and some other minor, less-soluble moieties. The mutual deliquescence transition was more distinct in Cl-depleted SSAs than in Cl-rich SSAs, suggesting that the eutonic component in the ambient SSAs is richer with other salts compared to NaCl. As RH increased further, both SSAs #23 and #11 underwent final deliquescence transitions at DRHs = 69.5%. The observed DRH for SSA #23 ($X_{(Na,Mg)Cl}$ = 0.52) is closer to the final DRH calculated from AIOMFAC for pure NaCl moiety in the Na(Cl, NO_3) system (Fig. 6), and higher than the AIOMFAC-calculated final DRH for pure NaCl moiety in the (Na, Mg)(Cl, NO_3) system (Figs. 5b and 6). The observed DRH for SSA #11 ($X_{(Na,Mg)Cl}$ = 0.23) is lower than the AIOMFAC-calculated final DRH (Fig. 6) for pure $NaNO_3$ moiety in the Na(Cl, NO_3) system (Gupta et al., 2015b), and close to the

AIOMFAC-calculated final DRH for pure $NaNO_3$ moiety in the (Na, Mg)(Cl, NO_3) system (Figs. 5e and 6). The observation of Cl-depleted SSAs during humidification suggests that a (Na, Mg)(Cl, NO_3) dominant composition drives the deliquescence transition. As RH increased further, the hygroscopic growth of both SSAs #23 and #11 was stunted, in comparison to the (Na, Mg)(Cl, NO_3) mixture systems (Figs. 5b and e), likely due to the presence of hydrophobic surfactants covering the aqueous salt droplet.

During the dehydration process, both SSAs #23 and #11 showed slower rates of shrinkage compared to the (Na, Mg)(Cl, NO_3) mixture systems (Figs. 5c and f), suggesting inhibition of water evaporation due to surface hydrophobic organic moieties. The diffraction patterns at the aqueous salt droplet-organic surfactant interface were more prominent in the form of color and/or ring-like patterns for equimolar and Cl-depleted SSAs (Figs. 5a and d), indicating that the hydrophobic organic film may become thicker, or the concentration of organic surfactants may increase with aging. During dehydration, SSA #23, which is equimolar or slightly Cl-rich, showed one sharp transition at RH = 44.1-43.6% and a gradual decrease in size thereafter until RH = 30.7%, which is not considered an efflorescence transition (Fig. 5a). The distinct ERH of 43.6% observed for SSA #23 was higher than the first ERHs of both Na(Cl, NO_3) and (Na, Mg)(Cl, NO_3) systems (Fig. 5c and 7), indicating possible homogeneous efflorescence of NaCl along with other salts on crystalline seeds such as (Ca, Na)SO_4 (Pósfai et al., 1995; Semeniuk et al., 2007; Wise et al., 2007), as shown in the X-ray maps in Fig. S5a. The remaining metastable amorphous/gel type NO_3^- moieties and $MgSO_4 \cdot xH_2O$ may be responsible for the gradual decrease in size after the efflorescence transition (Li et al., 2016). Cl-depleted SSA #11 showed two clear efflorescence transitions at RH = 44.1–39.6% and 24.6–23.9%, as shown in Fig. 5d. The first ERH of 39.6% measured for SSA #11 was also higher than the ERHs for both Na(Cl, NO_3) and (Na, Mg)(Cl, NO_3) systems, while the second ERH of 23.9% was close to and lower than the ERH range for pure NaCl in (Na, Mg)(Cl, NO_3) and Na(Cl, NO_3) systems, respectively (Figs. 5f and 7). The observations for Cl-depleted SSA #11 suggest that the first ERH was most probably due to the heterogeneous crystallization of the dominant $NaNO_3$ and/or $Mg(NO_3)_2$ on mixed cation sulfate crystalline seeds such as (Ca, Na)SO_4, while NaCl continued to homogeneously nucleate until the second ERH, where it crystallized at the center/core of the particle (Woods et al., 2013), as shown in the X-ray maps in Fig. S5b.

3.2.3 Phase diagrams of ambient SSAs in correlation with Na(Cl, NO_3) and (Na, Mg)(Cl, NO_3) surrogates systems

The phase diagrams of ambient SSAs in correlation with Na(Cl, NO_3) and (Na, Mg)(Cl, NO_3) surrogate systems can show the relationship between the observed deliquescence and efflorescence behavior of the ambient SSAs and those of the two surrogate systems. The ambient SSAs have more complex compositions, but the simpler Na(Cl, NO_3) and (Na, Mg)(Cl, NO_3) surrogate systems can help to identify the dominant salts and their behavior in the ambient SSAs. For example, the observation of Cl-depleted SSAs during humidification suggests that a (Na, Mg)(Cl, NO_3) dominant composition drives the deliquescence transition. This information can be useful in understanding the hygroscopic properties and behavior of atmospheric aerosols.

3.2.3.1 Deliquescence phase diagram

Fig. 6 shows the experimentally measured DRHs for the ambient SSA particles and those of the (Na, Mg)(Cl, NO_3) and Na(Cl, NO_3) systems, calculated from the AIOMFAC model, plotted as a function of the mole fraction of chloride, f($X_{(Na, Mg)Cl}$ or X_{NaCl}).

The first MDRH of the (Na, Mg)(Cl, NO_3) system, which was calculated from AIOMFAC, is 34.2%, and the MDRH measured in laboratory-generated (Na, Mg)(Cl, NO_3) particles is ~33.4% (Fig. S3). These values are attributed to the dominant $MgCl_2 \cdot 6H_2O$ eutonic component (Gupta et al., 2015a). In some Cl-rich SSAs, a gradual increase in size and a change in morphology were observed at RH = ~33%, indicating that they were in the partial aqueous phase (Figs. 4a and d). It is also possible that the gradual water uptake observed in SSAs at low RHs is due to amorphous inorganic moieties such as $MgSO_4 \cdot xH_2O$ (Xiao et al., 2008; Zhao et al., 2006) and $Mg(NO_3)_2 \cdot xH_2O$ (Zhang et al., 2004), and/or water-soluble secondary organics such as carboxylate salts formed due to reactions of the (Na, Mg)Cl species with dicarboxylic acids, which are ubiquitous in the marine boundary layer (Ghorai et al., 2014; Laskin et al., 2012; Li et al., 2021). Wise et al. (2009) reported that ambient SSAs started changing in morphology at 36(±15)% RH.

For the (Na, Mg)(Cl, NO_3) system, the eutonic composition is $X_{(Na,Mg)Cl}$ = 0.46, with a second MDRH of 66.5%, calculated from AIOMFAC, and a measured value of ~66.6(±0.4)% in the laboratory-generated (Na, Mg)(Cl, NO_3) particles (Fig. S3). For the Na(Cl, NO_3) system, the eutonic composition is X_{NaCl} = 0.38, with the MDRH of 67.9%, calculated from AIOMFAC, and a measured value of ~67.9(±0.3)% in the laboratory-generated particles (Gupta et al., 2015b). The observed MDRH of 63.8(±0.3)% for the ambient SSAs (Fig. 6) is slightly lower than those of the Na(Cl, NO_3) and (Na, Mg)(Cl, NO_3) mixture systems, indicating that the eutonic component in the mutual deliquescence

transition may be Na(Cl, NO_3)-rich, with minor concentrations of other soluble salt moieties, as the MDRH of salt mixtures is generally lower than individual salt DRHs (Wexler and Seinfeld, 1991). It is less likely that Na_2SO_4 or CH_3SO_3Na are major components of the eutonic component in these ambient SSAs, as they have much higher MDRHs, i.e., MDRHs = 84.0% for Na(Cl, SO_4) and 71% for Na(Cl, CH_3SO_3) (Chang and Lee, 2002; Liu and Laskin, 2009; Liu et al., 2011). The lowest final DRH measured for SSA #1 with $X_{(Na,Mg)Cl}$ = 0.33 is at RH = 65.4 % (Fig. 6), which is close to the observed MDRH of 63.8(±0.3)%, suggesting that the eutonic component likely has a chloride mole fraction within the range of $X_{(Na,Mg)Cl}$ = ~0.30–0.40. Interestingly, Wise et al. (2009) reported rounding in particle morphology at RH = 65(±4)%, which is close to the observed MDRH but was not confirmed as such since only four ambient SSA particles were studied.

The final DRHs in both (Na, Mg)(Cl, NO_3) and Na(Cl, NO_3) systems are solely determined by the solid salt remaining after the mutual deliquescence of the eutonic component. Fig. 6 clearly shows that for the Cl-rich SSA particles with $X_{(Na,Mg)Cl} > 0.40$, which contain more NaCl than the eutonic composition, the final DRH values (~67.5-73.5%) approached the DRH of pure NaCl salt (~75.3% at 298 K) as the chloride concentration increased. Similarly, for the Cl-depleted particles with $X_{(Na,Mg)Cl} <$ 0.40, the final DRH values (~65.4-72.9%) approached that of pure $NaNO_3$ salt (~74% at 298 K) as the chloride concentration decreased.

The chemical components of each phase in the ambient SSAs during the humidification process are not well known, therefore, five possible single and/or mixed phases are notated as alphabets (P, Q, R, S, and T) and the possible major chemical components in each phase (s = solid; aq = aqueous) are listed as follows:

(i) P-(s): all components are mixed in solid phase at RH < ~33–35% at all mole fractions of chloride.

(ii) Q-(s + aq): a mixed phase comprising possibly aqueous $MgCl_2 \cdot 6H_2O$ dominant eutonic components + solid NaCl, (Na, Mg, Ca)(NO_3, SO_4) and organics between RH = ~33% and the first clear MDRH of ~63.8%.

(iii) R-(s + aq): a mixed phase comprising solid $NaNO_3$ and (Ca, Na)SO_4 + aqueous eutonic components rich in Na(Cl, NO_3) and Mg(NO_3, SO_4, organics) between RH = 63.8% and final DRHs for $X_{(Na,Mg)Cl} < 0.40$, i.e., Cl-depleted SSAs.

(iv) S-(s + aq): a mixed phase comprising solid NaCl and (Ca, Na)SO_4 + aqueous eutonic components rich in Na(Cl ,NO_3) and Mg(Cl, NO_3, SO_4, organics) between the RH = 63.8% and

final DRHs for $X_{(Na,Mg)Cl} > 0.40$, i.e., Cl-rich SSAs.

(v) T-(aq): aqueous phase for most components including NaCl, $NaNO_3$, and Mg(Cl, NO_3, SO_4, organics) above the measured final DRHs at all mole fractions of chloride, while (Ca, Na)SO_4 should remain in crystalline solid phase and does not take part in the deliquescence transitions in the measured RH range.

3.2.3.2 Efflorescence phase diagram

The experimentally measured ERHs for the ambient SSA particles and those of (Na, Mg)(Cl, NO_3) and Na(Cl, NO_3) systems are plotted as a function of the mole fraction of chloride, f($X_{(Na,Mg)Cl}$ or X_{NaCl}) in Fig. 7.

The first ERH values decrease from 44.5% to 24.8% and from 47.1% to 20.2% with decreasing mole fractions of chloride for $X_{(Na, Mg)Cl} = 0.75$ to 0.25 in the (Na, Mg)(Cl, NO_3) and $X_{NaCl} = 0.9$ to 0.1 in the Na(Cl, NO_3) systems, respectively (Gupta et al., 2015b; Woods et al., 2013). This suggests that the first efflorescence transitions in the Na(Cl, NO_3) and (Na, Mg)(Cl, NO_3) mixture systems are solely due to the homogeneous nucleation of NaCl for both Cl-rich and Cl-depleted particles, and that the amorphous (Na, Mg)NO_3 species cannot undergo homogeneous crystallization even at high supersaturation (Kim et al., 2012; Zhang et al., 2004). In the case of Cl-rich ($X_{(Na,Mg)Cl} > 0.40$) ambient SSAs, the first ERHs systematically decreased ranging from 50.5% to 33.0% due to the homogeneous nucleation of NaCl for most particles. However, for a few particles, such as SSA #5 (Fig. 4a, ERH = 50.5%), NaCl underwent heterogeneous crystallization on the mixed cation sulfate (Ca, Na)SO_4 crystalline seeds, resulting in higher ERH values. On the other hand, in Cl-depleted ($X_{(Na,Mg)Cl} < 0.40$) SSA particles, the first ERH values ranged from 46.0% to 24.6% as a random set of values higher than the first ERHs in Na(Cl, NO_3) and (Na, Mg)(Cl, NO_3) mixture systems (Fig. 7), indicating heterogeneous crystallization of the richer (Na, Mg)NO_3 moieties on the mixed cation sulfate crystalline seeds for most particles.

The second/final ERH in the Na(Cl, NO_3) system was only observed for Cl-rich particles ($X_{NaCl} > 0.38$) due to the mutual efflorescence of the eutonic component ($X_{NaCl} = 0.38$) at MERH = ~30.0–35.5%, while no second ERH was recorded for Cl-depleted particles as $NaNO_3$ heterogeneously crystallized simultaneously on the homogeneously nucleated NaCl seeds (Gupta et al., 2015a). For the (Na, Mg)(Cl, NO_3), a second ERH = ~29.6–27.4% was only observed for $X_{(Na, Mg)Cl} = 0.5$ among the

three compositions measured (Fig. S3), probably due to the stochastic heterogeneous crystallization of the Na(Cl, NO_3)-rich eutonic moiety on the NaCl seed. On the other hand, the typical transitions from 30.5% to 17.9% for the second/final ERH in ambient SSAs were only observed for Cl-depleted particles with decreasing chloride concentration, i.e. $X_{(Na,\ Mg)Cl}$ = ~0.33 to 0.15, indicating homogeneous nucleation of NaCl followed by assumed simultaneous heterogeneous crystallization of remaining aqueous salt moieties such as Mg(SO_4, NO_3).

In the laboratory-generated (Na, Mg)(Cl, NO_3) particles with different mole fractions of chloride, i.e. $X_{(Na,\ Mg)Cl}$ = 0.25, 0.5, 0.75 (Fig. S3), and 1.0 (Gupta et al., 2015a), clear final ERHs or MERHs were observed at low RHs ranging in 11.0–5.1% ($X_{(Na,\ Mg)Cl}$ = 0.25, 0.5, and 1.0) and 14.6–12.1% ($X_{(Na,\ Mg)Cl}$ = 0.75), probably due to the crystallization of the dominant eutonic component of $MgCl_2 \cdot 4H_2O$ and $MgCl_2 \cdot 6H_2O$, respectively. However, such low values of ERHs were not observed in the ambient SSAs, possibly because the concentrations of $MgCl_2 \cdot xH_2O$ were too small to be detected by the optical microscopy-derived 2-D area ratio. On the other hand, the very gradual shrinkage observed in ambient SSAs at low RHs may be due to the presence of amorphous Mg(NO_3, SO_4)$\cdot xH_2O$ moieties, which were present in some particles (e.g., SSAs #5, #19, and #23 in Figs. 4a, 4d, and 5a).

Considering the possibility of water content at low RHs during the dehydration process (Cziczo et al., 1997; Gupta et al., 2015a; Tang et al., 1997), the ambient SSAs can be divided into five potential phases, denoted as alphabets (P, Q, R, S, T), based on the presence of different chemical components and their states at different relative humidities (RHs) and the major chemical components in each phase (s = solid; aq = aqueous) are listed as follows:

(i) P-(aq): Almost all components, including NaCl, $NaNO_3$, and Mg(Cl, NO_3, SO_4, organics), are mixed in the aqueous phase at RH > ~55% for all mole fractions of chloride. The (Ca, Na)SO_4 should remain in the crystalline solid phase as it does not take part in the phase transitions within the measured RH range.

(ii) Q-(s + aq): a mixed phase including solid NaCl and other heterogeneously crystallized moieties + aqueous nucleating species like $(Mg \cdot xH_2O)^{2+}$ and $Cl^-/NO_3^-/SO_4^{2-}$ at RHs < 50.5% in Cl-rich SSAs ($X_{(Na,\ Mg)Cl}$ > 0.40).

(iii) R-(s + aq): a mixed phase including heterogeneously crystallized (Na, Mg)$NO_3 \cdot xH_2O$ on crystalline (Ca, Na)$SO_4(xH_2O)$ seeds + aqueous NaCl and other moieties, between the first ERHs = 46.0–24.6% and final ERHs = 30.5–17.9% for Cl-depleted SSAs ($X_{(Na,\ Mg)Cl}$ < 0.40).

(iv) S-(s + aq): a mixed phase including solid (Na, Mg, Ca)(NO_3, SO_4)·xH_2O and homogeneously crystallized NaCl + aqueous/amorphous $(Mg \cdot xH_2O)^{2+}$ and NO_3^-/SO_4^{2-}, and other minor species below final ERHs = 30.5–17.9% for Cl-depleted SSAs ($X_{(Na, Mg)Cl} < 0.40$).

(v) T-(s): All components are mixed in solid phase at RH = ~14.6–5.0% for all mole fractions of chloride. Amorphous or gel forming Mg(NO_3, SO_4)·xH_2O shows gradual water loss, while only a small amount of $MgCl_2 \cdot xH_2O$ is expected to crystallize.

3.3 Non-SSA particles

Generally, mineral particles such as aluminosilicates and calcium carbonate tend to be difficult to absorb water and grow in size with increasing RH. However, these particles can become hygroscopic after reaction with NO_x and SO_2 in the presence of water and/or mixing with SSAs. Particle #14 shown in Fig. 8 is a highly aged aluminosilicate that has mixed with an SSA moiety, probably with (Na, Mg)(Cl, NO_3) and organic species as confirmed using X-ray spectrum. Clear deliquescence and efflorescence transitions are observed in the gradual growth and shrinkage of particle #14 due mainly to the SSA part, and the growth of the aged aluminosilicate is certainly smaller than the SSA at maximum RH. Particle #20 shown in Fig. S6 is a reacted Ca-containing particle with nitrate showing gradual change in size during humidification and dehydration processes, following hygroscopic property reported before (Ahn et al., 2010). Particle #36 is a typical ammonium sulfate mixed with organic species as shown in Fig. S7, and the major chemical components of particle #36 are C, N, O, and S. The particle showed a first partial deliquescence transition at RH = 67.5%, which may be the MDRH for the mixture of ammonium sulfate and organic species. Upon further increase in RH, the particle absorbed more moisture and fully dissolved at RH = 77.1%, which is slightly lower than the DRH of pure ammonium sulfate particles (Wu et al., 2019). During the dehydration process, particle #36 showed a slower rate of shrinkage than ammonium sulfate particles, indicating inhibition of water evaporation due to surface hydrophobic organic moieties, and effloresced at RH = 27.6%, which is lower than the ERH of ammonium sulfate particles (Wu et al., 2019). Some particles, such as reacted Ca-containing particles #17 and #25 and an aged SiO_2 particle #37, exhibit partial dissolution as shown in Fig. S8 and S9. The 2-D area ratio of particle #17 at maximum RH is larger than that of particle #25, indicating the existence of more hygroscopic components in particle #17. Particle #37 showed gradual increase and decrease with partial dissolution only on the right side of particle, possibly due to the reacted Ca-containing one with nitrate moiety. The observation of the hygroscopic behavior of particles having partial growth suggests that a

554 small content of hygroscopic chemical species can control the hygroscopic behavior of particles with
555 major non-hygroscopic species. On the other hand, genuine aluminosilicate particles #29 and #32 (Fig.
556 S10) and Fe-rich particles #2 and #7 (Fig. S11) did not show hygroscopic growth with changing RH.
557
558 **4 Atmospheric Implications**
559 The investigation of the hygroscopic behavior of ambient SSAs is crucial for understanding the
560 atmospheric chemistry and physics of marine environments. Previous studies have recognized that
561 SSAs contain a wide range of inorganic sea salt and organic species (Schiffer et al., 2018), making it
562 difficult to assess their hygroscopicity. In this study, the hygroscopic behavior of SSAs was
563 systematically characterized and correlated with the role of inorganic salt moieties and enriched organic
564 material coating. It was found that SSAs partially dissolve at lower RHs than the inorganic surrogates,
565 including (Na, Mg)(Cl, NO_3), due to the coexistence with other soluble moieties such as water-soluble
566 secondary organics. This indicates that SSAs will be increasingly susceptible to trace gas species and
567 subsequent heterogeneous chemical reactions (Lee et al., 2020). The degree of chloride depletion was
568 also found to affect the hygroscopic behavior of aged SSAs. SSAs with a higher degree of chloride
569 depletion, i.e., higher aging degree, tend to exhibit multiple phase transitions with reducing RH,
570 retaining phase-separated core-shell mixing state, which impacts aerosol-radiation interactions (Sun et
571 al., 2018). The importance of considering these surrogate systems when modeling the hygroscopic
572 behavior of ambient SSAs is apparent, especially in the case of field observations where a wide range
573 of mixing states exist in particles. Even though there are still discrepancies regarding whether the
574 organic fraction can influence the hygroscopic growth of SSAs, this study demonstrated that organic
575 substances covering the sea salt moieties did suppress their hygroscopic growth. Further investigations,
576 including obtaining exact elemental and molecular compositions of the organic shells, are needed to
577 examine the aging of SSAs and quantify their uncertain effects on SSAs' hygroscopicity in
578 thermodynamic models.
579 In addition, other species involving mineral dust and anthropogenic particles can be transported
580 into marine environments and mixed with SSAs, which alter the particle compositions and in turn, their
581 hygroscopicity. Heterogeneous mixing or coating of SSAs onto less hygroscopic dust particles can
582 enhance their ability to interact with water vapor and reactive trace gases, leading to the formation of
583 new particles and increased CCN activity (Tang et al., 2016). This mixing can also affect the optical
584 properties and radiative forcing of atmospheric aerosols, as the scattering and absorption of solar

585 radiation by aerosols are dependent on their size, composition, and mixing state. Furthermore, the
586 impact of anthropogenic emissions on the hygroscopicity of marine aerosols is an important area of
587 research, as increased levels of atmospheric pollutants may enhance the aerosol-water interaction and
588 lead to changes in cloud properties and precipitation patterns (Su et al., 2022). Therefore, a
589 comprehensive understanding of the hygroscopic behavior of marine aerosols and their interactions
590 with other atmospheric constituents is necessary for accurately predicting their impacts on climate and
591 air quality.
592
593 **5 Conclusions**
594 The hygroscopic behavior of individual ambient aerosol particles collected at a coastal site of
595 Jeju Island, Korea, was investigated in correlation with their chemical compositions derived from X-
596 ray microanalysis. Specifically, we focused on the hygroscopic behavior of ambient aged SSAs and
597 their dependence on the extent of reaction between Cl^- and NO_3^- ions, estimated from the mixing ratios
598 of these ions using SEM-EDX. The phase transitions of the aged SSAs were found to be dominated by
599 inorganics involving Na(Cl, NO_3) and/or (Na, Mg)(Cl, NO_3) systems, with organic surfactant films
600 covering the droplets suppressing hygroscopic growth and shrinkage with changing RH. For Cl-rich
601 SSAs, two major transitions were observed during the humidification process, firstly at the MDRH and
602 secondly at a final DRH. During the dehydration process, Cl-rich SSAs showed single-stage
603 efflorescence. Cl-depleted SSAs showed two prompt deliquescence transitions during the
604 humidification process and stepwise transitions during the dehydration process, depending on their
605 chemical compositions.
606 The hygroscopic behavior of other particle types, including aged aluminosilicate, Ca-containing,
607 organic and ammonium sulfate mixture, and Fe-rich particles, was also observed. Aged mineral
608 particles showed varying degrees of size changes with changing RH, potentially due to the presence of
609 SSAs and/or NO_3^- species resulting from coagulation and heterogeneous reactions, while non-reacted
610 mineral and Fe-rich particles did not exhibit significant size changes during the hygroscopic process.
611 The mixture particles of organic and ammonium sulfate displayed lower DRH and ERH values
612 compared to pure ammonium sulfate salt, indicating the impact of organic species on the hygroscopic
613 behavior of ammonium sulfate. While there have been some studies on the hygroscopic behavior of
614 ambient marine aerosols, this study is one of the first to systematically investigate their hygroscopic

behavior and to correlate it with their chemical compositions, providing better insights into their impact on climate change and atmospheric chemistry.

Data availability

The data used in this study are available upon request; please contact Chul-Un Ro (curo@inha.ac.kr).

Author contributions

LW, HJE, HY, DG, and HRC designed the experiment. LW, HJE, HY, and HRC carried out the measurements and/or analyzed the data. LW, HJE, HY, DG, HRC, PF, and CUR contributed discussion of the data. LW, HJE, DG, and CUR drafted the paper.

Competing interests

The authors declare that they have no conflict of interest.

Acknowledgements

This study was supported by the National Research Foundation of Korea (NRF) grant funded by the Korean government (MSIT) (No. 2021R1A4A1032579 and No. 2021R1A2C2004240) and by the National Institute of Environmental Research (NIER) funded by the Ministry of Environment (MOE) of Korea (NIER-2021-03-03-007).

References

Ahn, K.-H., Kim, S.-M., Jung, H.-J., Lee, M.-J., Eom, H.-J., Maskey, S., and Ro, C.-U.: Combined Use of Optical and Electron Microscopic Techniques for the Measurement of Hygroscopic Property, Chemical Composition, and Morphology of Individual Aerosol Particles, Anal. Chem., 82, 7999-8009, 10.1021/ac101432y, 2010.

Ansari, A. S. and Pandis, S. N.: Prediction of multicomponent inorganic atmospheric aerosol behavior, Atmos. Environ., 33, 745-757, http://dx.doi.org/10.1016/S1352-2310(98)00221-0, 1999.

Atkinson, D. B., Radney, J. G., Lum, J., Kolesar, K. R., Cziczo, D. J., Pekour, M. S., Zhang, Q., Setyan, A., Zelenyuk, A., and Cappa, C. D.: Aerosol optical hygroscopicity measurements during the 2010 CARES campaign, Atmos. Chem. Phys, 15, 4045-4061, 10.5194/acp-15-4045-2015, 2015.

Ault, A. P., Guasco, T. L., Baltrusaitis, J., Ryder, O. S., Trueblood, J. V., Collins, D. B., Ruppel, M. J., Cuadra-Rodriguez, L. A., Prather, K. A., and Grassian, V. H.: Heterogeneous Reactivity of Nitric Acid with Nascent Sea Spray Aerosol: Large Differences Observed between and within Individual Particles, J. Phys. Chem. Lett, 5, 2493-2500, 10.1021/jz5008802, 2014.

Ault, A. P., Moffet, R. C., Baltrusaitis, J., Collins, D. B., Ruppel, M. J., Cuadra-Rodriguez, L. A., Zhao, D., Guasco, T. L., Ebben, C. J., Geiger, F. M., Bertram, T. H., Prather, K. A., and Grassian, V. H.:

Size-Dependent Changes in Sea Spray Aerosol Composition and Properties with Different Seawater Conditions, Environ. Sci. Technol., 47, 5603-5612, 10.1021/es400416g, 2013.
Beardsley, R., Jang, M., Ori, B., Im, Y., Delcomyn, C. A., and Witherspoon, N.: Role of sea salt aerosols in the formation of aromatic secondary organic aerosol: yields and hygroscopic properties, Environ. Chem., 10, 167-177, http://dx.doi.org/10.1071/EN13016, 2013.
Bertram, T. H., Cochran, R. E., Grassian, V. H., and Stone, E. A.: Sea spray aerosol chemical composition: elemental and molecular mimics for laboratory studies of heterogeneous and multiphase reactions, Chem. Soc. Rev., 47, 2374-2400, 10.1039/c7cs00008a, 2018.
Carslaw, K. S., Clegg, S. L., and Brimblecombe, P.: A Thermodynamic Model of the System HCl-HNO3-H2SO4-H2O, Including Solubilities of HBr, from < 200 to 328 K, J. Phys. Chem. A, 99, 11557-11574, 10.1021/j100029a039, 1995.
Chan, C. K., Ha, Z., and Choi, M. Y.: Study of water activities of aerosols of mixtures of sodium and magnesium salts, Atmos. Environ., 34, 4795-4803, 10.1016/S1352-2310(00)00252-1, 2000.
Chan, C. K., Liang, Z., Zheng, J., Clegg, S. L., and Brimblecombe, P.: Thermodynamic properties of aqueous aerosols to high supersaturation: I—measurements of water activity of the system $Na^+–Cl^––NO_3^––SO_4^{2–}–H_2O$ at~ 298.15 K, Aerosol Sci. Technol., 27, 324-344, 10.1080/02786829708965477, 1997.
Chang, S.-Y. and Lee, C.-T.: Applying GC-TCD to investigate the hygroscopic characteristics of mixed aerosols, Atmos. Environ., 36, 1521-1530, 10.1016/S1352-2310(01)00546-5, 2002.
Clegg, S. L., Brimblecombe, P., and Wexler, A. S.: Thermodynamic Model of the System $H^+–NH_4^+–Na^+–SO_4^{2-}–NO_3^-–Cl^-–H_2O$ at 298.15 K, J. Phys. Chem. A, 102, 2155-2171, 10.1021/jp973043j, 1998a.
Clegg, S. L., Brimblecombe, P., and Wexler, A. S.: Thermodynamic Model of the System $H^+–NH_4^+–SO_4^{2-}–NO_3^-–H_2O$ at Tropospheric Temperatures, J. Phys. Chem. A, 102, 2137-2154, 10.1021/jp973042r, 1998b.
Cochran, R. E., Laskina, O., Jayarathne, T., Laskin, A., Laskin, J., Lin, P., Sultana, C., Lee, C., Moore, K. A., Cappa, C. D., Bertram, T. H., Prather, K. A., Grassian, V. H., and Stone, E. A.: Analysis of Organic Anionic Surfactants in Fine and Coarse Fractions of Freshly Emitted Sea Spray Aerosol, Environ. Sci. Technol., 50, 2477-2486, 10.1021/acs.est.5b04053, 2016.
Cochran, R. E., Laskina, O., Trueblood, J. V., Estillore, A. D., Morris, H. S., Jayarathne, T., Sultana, C. M., Lee, C., Lin, P., Laskin, J., Laskin, A., Dowling, J. A., Qin, Z., Cappa, C. D., Bertram, T. H., Tivanski, A. V., Stone, E. A., Prather, K. A., and Grassian, V. H.: Molecular Diversity of Sea Spray Aerosol Particles: Impact of Ocean Biology on Particle Composition and Hygroscopicity, Chem, 2, 655-667, 10.1016/j.chempr.2017.03.007, 2017.
Cohen, M. D., Flagan, R. C., and Seinfeld, J. H.: Studies of concentrated electrolyte solutions using the electrodynamic balance. 3. Solute nucleation, J. Phys. Chem, 91, 4583-4590, 10.1021/j100301a031, 1987.
Cziczo, D. J., Nowak, J. B., Hu, J. H., and Abbatt, J. P. D.: Infrared spectroscopy of model tropospheric aerosols as a function of relative humidity: Observation of deliquescence and crystallization, J. Geophys. Res. Atmos., 102, 18843-18850, 10.1029/97jd01361, 1997.
Eom, H.-J., Gupta, D., Li, X., Jung, H.-J., Kim, H., and Ro, C.-U.: Influence of Collecting Substrates on the Characterization of Hygroscopic Properties of Inorganic Aerosol Particles, Anal. Chem., 86, 2648-2656, 10.1021/ac4042075, 2014.
Eom, H. J., Gupta, D., Cho, H. R., Hwang, H., Hur, S., Gim, Y., and Ro, C. U.: Single-particle investigation of summertime and wintertime Antarctic sea spray aerosols using low-Z particle

EPMA, Raman microspectrometry, and ATR-FTIR imaging techniques, Atmos. Chem. Phys., 2016, 1-30, 10.5194/acp-2016-584, 2016.
Finlayson-Pitts, B. J. and Pitts, J. N.: Chemistry of the upper and lower atmosphere : theory, experiments, and applications, Academic Press, San Diego, 2000.
Forestieri, S. D., Cornwell, G. C., Helgestad, T. M., Moore, K. A., Lee, C., Novak, G. A., Sultana, C. M., Wang, X., Bertram, T. H., Prather, K. A., and Cappa, C. D.: Linking variations in sea spray aerosol particle hygroscopicity to composition during two microcosm experiments, Atmos. Chem. Phys., 16, 9003-9018, 10.5194/acp-16-9003-2016, 2016.
Freney, E. J., Adachi, K., and Buseck, P. R.: Internally mixed atmospheric aerosol particles: Hygroscopic growth and light scattering, J. Geophys. Res. Atmos., 115, D19210, 10.1029/2009jd013558, 2010.
Gard, E. E., Kleeman, M. J., Gross, D. S., Hughes, L. S., Allen, J. O., Morrical, B. D., Fergenson, D. P., Dienes, T., E. Gälli, M., and Johnson, R. J.: Direct observation of heterogeneous chemistry in the atmosphere, Science, 279, 1184-1187, 10.1126/science.279.5354.1184, 1998.
Ge, Z., Wexler, A. S., and Johnston, M. V.: Multicomponent Aerosol Crystallization, J. Colloid Interface Sci., 183, 68-77, http://dx.doi.org/10.1006/jcis.1996.0519, 1996.
Ge, Z., Wexler, A. S., and Johnston, M. V.: Deliquescence Behavior of Multicomponent Aerosols, J. Phys. Chem. A, 102, 173-180, 10.1021/jp972396f, 1998.
Geng, H., Hwang, H., Liu, X., Dong, S., and Ro, C. U.: Investigation of aged aerosols in size-resolved Asian dust storm particles transported from Beijing, China, to Incheon, Korea, using low-Z particle EPMA, Atmos. Chem. Phys., 14, 3307-3323, 10.5194/acp-14-3307-2014, 2014.
Geng, H., Kang, S., Jung, H. J., Choël, M., Kim, H., and Ro, C. U.: Characterization of individual submicrometer aerosol particles collected in Incheon, Korea, by quantitative transmission electron microscopy energy-dispersive X-ray spectrometry, J. Geophys. Res. Atmos., 115, 10.1029/2009JD013486, 2010.
Ghorai, S., Wang, B., Tivanski, A., and Laskin, A.: Hygroscopic properties of internally mixed particles composed of NaCl and water-soluble organic acids, Environ. Sci. Technol., 48, 2234-2241, 10.1021/es404727u, 2014.
Guo, L., Gu, W., Peng, C., Wang, W., Li, Y. J., Zong, T., Tang, Y., Wu, Z., Lin, Q., Ge, M., Zhang, G., Hu, M., Bi, X., Wang, X., and Tang, M.: A comprehensive study of hygroscopic properties of calcium- and magnesium-containing salts: implication for hygroscopicity of mineral dust and sea salt aerosols, Atmos. Chem. Phys, 19, 2115-2133, 10.5194/acp-19-2115-2019, 2019.
Gupta, D., Eom, H. J., Cho, H. R., and Ro, C. U.: Hygroscopic behavior of NaCl–$MgCl_2$ mixture particles as nascent sea-spray aerosol surrogates and observation of efflorescence during humidification, Atmos. Chem. Phys., 15, 11273-11290, 10.5194/acp-15-11273-2015, 2015a.
Gupta, D., Kim, H., Park, G., Li, X., Eom, H. J., and Ro, C. U.: Hygroscopic properties of NaCl and $NaNO_3$ mixture particles as reacted inorganic sea-salt aerosol surrogates, Atmos. Chem. Phys., 15, 3379-3393, 10.5194/acp-15-3379-2015, 2015b.
Haynes, W. M.: CRC Handbook of Chemistry and Physics, 96th Edition, CRC Press, Boca Raton, Florida, 14–18, 2015.
Haywood, J. and Boucher, O.: Estimates of the direct and indirect radiative forcing due to tropospheric aerosols: A review, Rev. Geophys., 38, 513-543, 10.1029/1999rg000078, 2000.
Herich, H., Kammermann, L., Friedman, B., Gross, D. S., Weingartner, E., Lohmann, U., Spichtinger, P., Gysel, M., Baltensperger, U., and Cziczo, D. J.: Subarctic atmospheric aerosol composition: 2. Hygroscopic growth properties, J. Geophys. Res. Atmos., 114, D13204, 10.1029/2008jd011574, 2009.

Keene, W. C., Maring, H., Maben, J. R., Kieber, D. J., Pszenny, A. A. P., Dahl, E. E., Izaguirre, M. A., Davis, A. J., Long, M. S., Zhou, X., Smoydzin, L., and Sander, R.: Chemical and physical characteristics of nascent aerosols produced by bursting bubbles at a model air-sea interface, J. Geophys. Res. Atmos., 112, D21202, 10.1029/2007jd008464, 2007.

Kim, H., Lee, M.-J., Jung, H.-J., Eom, H.-J., Maskey, S., Ahn, K.-H., and Ro, C.-U.: Hygroscopic behavior of wet dispersed and dry deposited NaNO3 particles, Atmos. Environ., 60, 68-75, http://dx.doi.org/10.1016/j.atmosenv.2012.06.011, 2012.

Kong, X., Wolf, M. J., Roesch, M., Thomson, E. S., Bartels-Rausch, T., Alpert, P. A., Ammann, M., Prisle, N. L., and Cziczo, D. J.: A continuous flow diffusion chamber study of sea salt particles acting as cloud nuclei: deliquescence and ice nucleation, Tellus B: Chem. Phys. Meteorol., 70, 1-11, 10.1080/16000889.2018.1463806, 2018.

Krieger, U. K., Marcolli, C., and Reid, J. P.: Exploring the complexity of aerosol particle properties and processes using single particle techniques, Chem. Soc. Rev., 41, 6631-6662, 10.1039/c2cs35082c, 2012.

Krueger, B. J., Grassian, V. H., Iedema, M. J., Cowin, J. P., and Laskin, A.: Probing Heterogeneous Chemistry of Individual Atmospheric Particles Using Scanning Electron Microscopy and Energy-Dispersive X-ray Analysis, Anal. Chem., 75, 5170-5179, 10.1021/ac034455t, 2003.

Laskin, A., Moffet, R. C., Gilles, M. K., Fast, J. D., Zaveri, R. A., Wang, B., Nigge, P., and Shutthanandan, J.: Tropospheric chemistry of internally mixed sea salt and organic particles: Surprising reactivity of NaCl with weak organic acids, J. Geophys. Res. Atmos., 117, Tropospheric chemistry of internally mixed sea salt and organic particles: Surprising reactivity of NaCl with weak organic acids, 2012.

Lee, H. D., Morris, H. S., Laskina, O., Sultana, C. M., Lee, C., Jayarathne, T., Cox, J. L., Wang, X., Hasenecz, E. S., DeMott, P. J., Bertram, T. H., Cappa, C. D., Stone, E. A., Prather, K. A., Grassian, V. H., and Tivanski, A. V.: Organic Enrichment, Physical Phase State, and Surface Tension Depression of Nascent Core–Shell Sea Spray Aerosols during Two Phytoplankton Blooms, ACS Earth Space Chem., 4, 650-660, 10.1021/acsearthspacechem.0c00032, 2020.

Li, X., Wu, L., Lee, J.-S., and Ro, C.-U.: Hygroscopic behavior and chemical reactivity of aerosols generated from mixture solutions of low molecular weight dicarboxylic acids and NaCl, Phys. Chem. Chem. Phys., 23, 11052-11064, 10.1039/d1cp00590a, 2021.

Li, X., Gupta, D., Eom, H.-J., Kim, H., and Ro, C.-U.: Deliquescence and efflorescence behavior of individual NaCl and KCl mixture aerosol particles, Atmos. Environ., 82, 36-43, http://dx.doi.org/10.1016/j.atmosenv.2013.10.011, 2014.

Li, Y. J., Liu, P. F., Bergoend, C., Bateman, A. P., and Martin, S. T.: Rebounding hygroscopic inorganic aerosol particles: Liquids, gels, and hydrates, Aerosol Sci. Technol., 51, 388-396, 10.1080/02786826.2016.1263384, 2016.

Liu, Y. and Laskin, A.: Hygroscopic Properties of CH_3SO_3Na, $CH_3SO_3NH_4$, $(CH_3SO_3)_2Mg$, and $(CH_3SO_3)_2Ca$ Particles Studied by micro-FTIR Spectroscopy, J. Phys. Chem. A, 113, 1531-1538, 10.1021/jp8079149, 2009.

Liu, Y., Cain, J. P., Wang, H., and Laskin, A.: Kinetic Study of Heterogeneous Reaction of Deliquesced NaCl Particles with Gaseous HNO_3 Using Particle-on-Substrate Stagnation Flow Reactor Approach, J. Phys. Chem. A, 111, 10026-10043, 10.1021/jp072005p, 2007.

Liu, Y., Minofar, B., Desyaterik, Y., Dames, E., Zhu, Z., Cain, J. P., Hopkins, R. J., Gilles, M. K., Wang, H., and Jungwirth, P.: Internal structure, hygroscopic and reactive properties of mixed sodium methanesulfonate-sodium chloride particles, Phys. Chem. Chem. Phys., 13, 11846-11857, 10.1039/C1CP20444K, 2011.

788 Martin, S. T.: Phase Transitions of Aqueous Atmospheric Particles, Chem. Rev., 100, 3403-3454,
789 10.1021/cr990034t, 2000.
790 Meskhidze, N., Petters, M. D., Tsigaridis, K., Bates, T., O'Dowd, C., Reid, J., Lewis, E. R., Gantt, B.,
791 Anguelova, M. D., Bhave, P. V., Bird, J., Callaghan, A. H., Ceburnis, D., Chang, R., Clarke, A.,
792 de Leeuw, G., Deane, G., DeMott, P. J., Elliot, S., Facchini, M. C., Fairall, C. W., Hawkins, L.,
793 Hu, Y., Hudson, J. G., Johnson, M. S., Kaku, K. C., Keene, W. C., Kieber, D. J., Long, M. S.,
794 Mårtensson, M., Modini, R. L., Osburn, C. L., Prather, K. A., Pszenny, A., Rinaldi, M., Russell, L.
795 M., Salter, M., Sayer, A. M., Smirnov, A., Suda, S. R., Toth, T. D., Worsnop, D. R., Wozniak, A.,
796 and Zorn, S. R.: Production mechanisms, number concentration, size distribution, chemical
797 composition, and optical properties of sea spray aerosols, Atmos. Sci. Lett., 14, 207-213,
798 10.1002/asl2.441, 2013.
799 Mikhailov, E., Vlasenko, S., Martin, S. T., Koop, T., and Pöschl, U.: Amorphous and crystalline aerosol
800 particles interacting with water vapor: conceptual framework and experimental evidence for
801 restructuring, phase transitions and kinetic limitations, Atmos. Chem. Phys, 9, 9491-9522,
802 10.5194/acp-9-9491-2009, 2009.
803 Ming, Y. and Russell, L. M.: Predicted hygroscopic growth of sea salt aerosol, J. Geophys. Res. Atmos.,
804 106, 28259-28274, 10.1029/2001jd000454, 2001.
805 Nguyen, Q. T., Kjær, K. H., Kling, K. I., Boesen, T., and Bilde, M.: Impact of fatty acid coating on the
806 CCN activity of sea salt particles, Tellus B: Chem. Phys. Meteorol., 69, 1304064,
807 10.1080/16000889.2017.1304064, 2017.
808 Niedermeier, D., Wex, H., Voigtländer, J., Stratmann, F., Brüggemann, E., Kiselev, A., Henk, H., and
809 Heintzenberg, J.: LACIS-measurements and parameterization of sea-salt particle hygroscopic
810 growth and activation, Atmos. Chem. Phys., 8, 579-590, 10.5194/acp-8-579-2008, 2008.
811 O'Dowd, C. D. and de Leeuw, G.: Marine aerosol production: a review of the current knowledge, Philos.
812 trans., Math. phys. eng. sci., 365, 1753-1774, 10.1098/rsta.2007.2043, 2007.
813 Pandis, S. N., Wexler, A. S., and Seinfeld, J. H.: Dynamics of Tropospheric Aerosols, J. Phys. Chem.,
814 99, 9646-9659, 10.1021/j100024a003, 1995.
815 Pöschl, U. and Shiraiwa, M.: Multiphase Chemistry at the Atmosphere–Biosphere Interface Influencing
816 Climate and Public Health in the Anthropocene, Chem. Rev., 115, 4440-4475, 10.1021/cr500487s,
817 2015.
818 Pósfai, M., Anderson, J. R., Buseck, P. R., and Sievering, H.: Compositional variations of sea-salt-mode
819 aerosol particles from the North Atlantic, J. Geophys. Res. Atmos., 100, 23063-23074,
820 10.1029/95jd01636, 1995.
821 Prather, K. A., Bertram, T. H., Grassian, V. H., Deane, G. B., Stokes, M. D., DeMott, P. J., Aluwihare,
822 L. I., Palenik, B. P., Azam, F., Seinfeld, J. H., Moffet, R. C., Molina, M. J., Cappa, C. D., Geiger,
823 F. M., Roberts, G. C., Russell, L. M., Ault, A. P., Baltrusaitis, J., Collins, D. B., Corrigan, C. E.,
824 Cuadra-Rodriguez, L. A., Ebben, C. J., Forestieri, S. D., Guasco, T. L., Hersey, S. P., Kim, M. J.,
825 Lambert, W. F., Modini, R. L., Mui, W., Pedler, B. E., Ruppel, M. J., Ryder, O. S., Schoepp, N. G.,
826 Sullivan, R. C., and Zhao, D.: Bringing the ocean into the laboratory to probe the chemical
827 complexity of sea spray aerosol, Proc. Natl. Acad. Sci. USA, 110, 7550-7555,
828 10.1073/pnas.1300262110, 2013.
829 Quinn, P. K., Collins, D. B., Grassian, V. H., Prather, K. A., and Bates, T. S.: Chemistry and Related
830 Properties of Freshly Emitted Sea Spray Aerosol, Chem. Rev., 10.1021/cr500713g, 2015.
831 Rosati, B., Christiansen, S., Dinesen, A., Roldin, P., Massling, A., Nilsson, E. D., and Bilde, M.: The
832 impact of atmospheric oxidation on hygroscopicity and cloud droplet activation of inorganic sea
833 spray aerosol, Sci. Rep., 11, 10008, 10.1038/s41598-021-89346-6, 2021.

Ryder, O. S., Ault, A. P., Cahill, J. F., Guasco, T. L., Riedel, T. P., Cuadra-Rodriguez, L. A., Gaston, C. J., Fitzgerald, E., Lee, C., Prather, K. A., and Bertram, T. H.: On the Role of Particle Inorganic Mixing State in the Reactive Uptake of N_2O_5 to Ambient Aerosol Particles, Environ. Sci. Technol., 48, 1618-1627, 10.1021/es4042622, 2014.

Saul, T. D., Tolocka, M. P., and Johnston, M. V.: Reactive Uptake of Nitric Acid onto Sodium Chloride Aerosols Across a Wide Range of Relative Humidities, J. Phys. Chem. A, 110, 7614-7620, 10.1021/jp060639a, 2006.

Schiffer, J. M., Mael, L. E., Prather, K. A., Amaro, R. E., and Grassian, V. H.: Sea Spray Aerosol: Where Marine Biology Meets Atmospheric Chemistry, ACS Cent. Sci., 4, 1617-1623, 10.1021/acscentsci.8b00674, 2018.

Schill, S. R., Collins, D. B., Lee, C., Morris, H. S., Novak, G. A., Prather, K. A., Quinn, P. K., Sultana, C. M., Tivanski, A. V., Zimmermann, K., Cappa, C. D., and Bertram, T. H.: The Impact of Aerosol Particle Mixing State on the Hygroscopicity of Sea Spray Aerosol, ACS Cent. Sci., 1, 132-141, 10.1021/acscentsci.5b00174, 2015.

Schindelholz, E., Risteen, B., and Kelly, R.: Effect of relative humidity on corrosion of steel under sea salt aerosol proxies: I. NaCl, J. Electrochem. Soc., 161, C450, 10.1149/2.0221410jes, 2014.

Seinfeld, J. H. and Pandis, S. N.: Atmospheric chemistry and physics: from air pollution to climate change, 2nd ed., J. Wiley, Hoboken NJ, 1203 pp., 2006.

Semeniuk, T. A., Wise, M. E., Martin, S. T., Russell, L. M., and Buseck, P. R.: Water uptake characteristics of individual atmospheric particles having coatings, Atmos. Environ., 41, 6225-6235, 10.1016/j.atmosenv.2007.04.001, 2007.

Song, Y., Li, J., Tsona, N. T., Liu, L., and Du, L.: Enrichment of short-chain organic acids transferred to submicron sea spray aerosols, Sci. Total Environ., 851, 158122, 10.1016/j.scitotenv.2022.158122, 2022.

Su, B., Wang, T., Zhang, G., Liang, Y., Lv, C., Hu, Y., Li, L., Zhou, Z., Wang, X., and Bi, X.: A review of atmospheric aging of sea spray aerosols: Potential factors affecting chloride depletion, Atmos. Environ., 290, 10.1016/j.atmosenv.2022.119365, 2022.

Sun, J., Liu, L., Xu, L., Wang, Y., Wu, Z., Hu, M., Shi, Z., Li, Y., Zhang, X., Chen, J., and Li W.,: Key role of nitrate in phase transitions of urban particles: implications of important reactive surfaces for secondary aerosol formation, J. Geophys. Res. Atmos., 123, 1234-1243, 10.1002/2017JD027264, 2018.

Tang, I. N., Tridico, A. C., and Fung, K. H.: Thermodynamic and optical properties of sea salt aerosols, J. Geophys. Res. Atmos., 102, 23269-23275, 10.1029/97jd01806, 1997.

Tang, M., Cziczo, D. J., and Grassian, V. H.: Interactions of water with mineral dust aerosol: water adsorption, hygroscopicity, cloud condensation, and ice nucleation, Chem. Rev., 116, 4205-4259, 10.1021/acs.chemrev.5b00529, 2016.

ten Brink, H. M.: Reactive uptake of HNO_3 and H_2SO_4 in sea-salt (NaCl) particles, J. Aerosol Sci., 29, 57-64, http://dx.doi.org/10.1016/S0021-8502(97)00460-6, 1998.

Tobon, Y. A., El Hajj, D., Seng, S., Bengrad, F., Moreau, M., Visez, N., Chiapello, I., Crumeyrolle, S., and Choel, M.: Impact of the particle mixing state on the hygroscopicity of internally mixed sodium chloride-ammonium sulfate single droplets: a theoretical and experimental study, Phys. Chem. Chem. Phys., 23, 14391-14403, 10.1039/d1cp01574e, 2021.

Vaishya, A., Ovadnevaite, J., Bialek, J., Jennings, S. G., Ceburnis, D., and O'Dowd, C. D.: Bistable effect of organic enrichment on sea spray radiative properties, Geophys. Res. Lett., 40, 6395-6398, 10.1002/2013gl058452, 2013.

Vekemans, B., Janssens, K., Vincze, L., Adams, F., and Van Espen, P.: Analysis of X-ray spectra by iterative least squares (AXIL): New developments, Xray Spectrom., 23, 278-285, 10.1002/xrs.1300230609, 1994.

Wang, J. and Martin, S. T.: Satellite characterization of urban aerosols: Importance of including hygroscopicity and mixing state in the retrieval algorithms, J. Geophys. Res. Atmos., 112, D17203, 10.1029/2006jd008078, 2007.

Wang, X., Sultana, C. M., Trueblood, J., Hill, T. C., Malfatti, F., Lee, C., Laskina, O., Moore, K. A., Beall, C. M., and McCluskey, C. S.: Microbial control of sea spray aerosol composition: A tale of two blooms, ACS Central Science, 1, 124-131, 10.1021/acscentsci.5b00148, 2015.

Wang, X., Deane, G. B., Moore, K. A., Ryder, O. S., Stokes, M. D., Beall, C. M., Collins, D. B., Santander, M. V., Burrows, S. M., Sultana, C. M., and Prather, K. A.: The role of jet and film drops in controlling the mixing state of submicron sea spray aerosol particles, Proc. Natl. Acad. Sci. USA, 114, 6978-6983, 10.1073/pnas.1702420114, 2017.

Wexler, A. S. and Clegg, S. L.: Atmospheric aerosol models for systems including the ions H^+, NH_4^+, Na^+, SO_4^{2-}, NO_3^-, Cl^-, Br^-, and H_2O, J. Geophys. Res. A, 107, D14, 4207, 10.1029/2001jd000451, 2002.

Wexler, A. S. and Seinfeld, J. H.: Second-generation inorganic aerosol model, Atmos. Environ., 27A, 25, 2731-2748, 10.1016/0960-1686(91)90203-J, 1991.

Wise, M. E., Semeniuk, T. A., Bruintjes, R., Martin, S. T., Russell, L. M., and Buseck, P. R.: Hygroscopic behavior of NaCl-bearing natural aerosol particles using environmental transmission electron microscopy, J. Geophys. Res. Atmos., 112, D10224, 10.1029/2006jd007678, 2007.

Wise, M. E., Freney, E. J., Tyree, C. A., Allen, J. O., Martin, S. T., Russell, L. M., and Buseck, P. R.: Hygroscopic behavior and liquid-layer composition of aerosol particles generated from natural and artificial seawater, J. Geophys. Res. Atmos., 114, D03201, 10.1029/2008jd010449, 2009.

Woods, E., Chung, D., Lanney, H. M., and Ashwell, B. A.: Surface Morphology and Phase Transitions in Mixed NaCl/MgSO4 Aerosol Particles, J. Phys. Chem. A, 114, 2837-2844, 10.1021/jp911133j, 2010.

Woods, E., Heylman, K. D., Gibson, A. K., Ashwell, A. P., and Rossi, S. R.: Effects of NOy Aging on the Dehydration Dynamics of Model Sea Spray Aerosol, J. Phys. Chem. A, 117, 4214-4222, 10.1021/jp401646d, 2013.

Wu, L., Li, X., and Ro, C.-U.: Hygroscopic Behavior of Ammonium Sulfate, Ammonium Nitrate, and their Mixture Particles, Asian J. Atmos., 13, 196-211, 10.5572/ajae.2019.13.3.196, 2019.

Wu, L., Becote, C., Sobanska, S., Flaud, P.-M., Perraudin, E., Villenave, E., Song, Y.-C., and Ro, C.-U.: Hygroscopic behavior of aerosols generated from solutions of 3-methyl-1,2,3-butanetricarboxylic acid, its sodium salts, and its mixtures with NaCl, Atmos. Chem. Phys., 20, 14103-14122, 10.5194/acp-20-14103-2020, 2020.

Xiao, H.-S., Dong, J.-L., Wang, L.-Y., Zhao, L.-J., Wang, F., and Zhang, Y.-H.: Spatially resolved micro-raman observation on the phase separation of effloresced sea salt droplets, Environ. Sci. Technol., 42, 8698-8702, 10.1021/es801181f, 2008.

Xu, W., Ovadnevaite, J., Fossum, K. N., Lin, C., Huang, R.-J., O'Dowd, C., and Ceburnis, D.: Aerosol hygroscopicity and its link to chemical composition in the coastal atmosphere of Mace Head: marine and continental air masses, Atmos. Chem. Phys, 20, 3777-3791, 10.5194/acp-20-3777-2020, 2020.

Zhang, X., Massoli, P., Quinn, P. K., Bates, T. S., and Cappa, C. D.: Hygroscopic growth of submicron and supermicron aerosols in the marine boundary layer, J. Geophys. Res. Atmos., 119, 8384-8399, 10.1002/2013jd021213, 2014.

Zhang, Y.-H., Choi, M. Y., and Chan, C. K.: Relating Hygroscopic Properties of Magnesium Nitrate to the Formation of Contact Ion Pairs, J. Phys. Chem. A, 108, 1712-1718, 10.1021/jp036524d, 2004.

Zhao, L.-J., Zhang, Y.-H., Wei, Z.-F., Cheng, H., and Li, X.-H.: Magnesium Sulfate Aerosols Studied by FTIR Spectroscopy: Hygroscopic Properties, Supersaturated Structures, and Implications for Seawater Aerosols, J. Phys. Chem. A, 110, 951-958, 10.1021/jp055291i, 2006.

Zieger, P., Vaisanen, O., Corbin, J. C., Partridge, D. G., Bastelberger, S., Mousavi-Fard, M., Rosati, B., Gysel, M., Krieger, U. K., Leck, C., Nenes, A., Riipinen, I., Virtanen, A., and Salter, M. E.: Revising the hygroscopicity of inorganic sea salt particles, Nat. Commun., 8, 15883, 10.1038/ncomms15883, 2017.

Zuend, A., Marcolli, C., Luo, B. P., and Peter, T.: A thermodynamic model of mixed organic-inorganic aerosols to predict activity coefficients, Atmos. Chem. Phys., 8, 4559–4593, 10.5194/acp-8-4559-2008, 2008.

Zuend, A., Marcolli, C., Booth, A. M., Lienhard, D. M., Soonsin, V., Krieger, U. K., Topping, D. O., McFiggans, G., Peter, T., and Seinfeld, J. H.: New and extended parameterization of the thermodynamic model AIOMFAC: calculation of activity coefficients for organic-inorganic mixtures containing carboxyl, hydroxyl, carbonyl, ether, ester, alkenyl, alkyl, and aromatic functional groups, Atmos. Chem. Phys., 11, 9155–9206, 10.5194/acp-11-9155-2011, 2011.

943 **Figure 1.** Location of Gosan sampling site on Jeju Island, South Korea. (Map Copyright © Google Earth)

944

945

Figure 2. (a) Secondary electron image (SEI) of the first field containing 16 particles and X-ray spectra of (b) a Cl-rich and (c) a Cl-depleted aged SSAs **(**particles #5 and #11, respectively)**.** In this image, aged SSAs, Fe-containing particles, and aluminosilicates are denoted as "r-SS", "Fe-rich", and "AlSi", respectively.

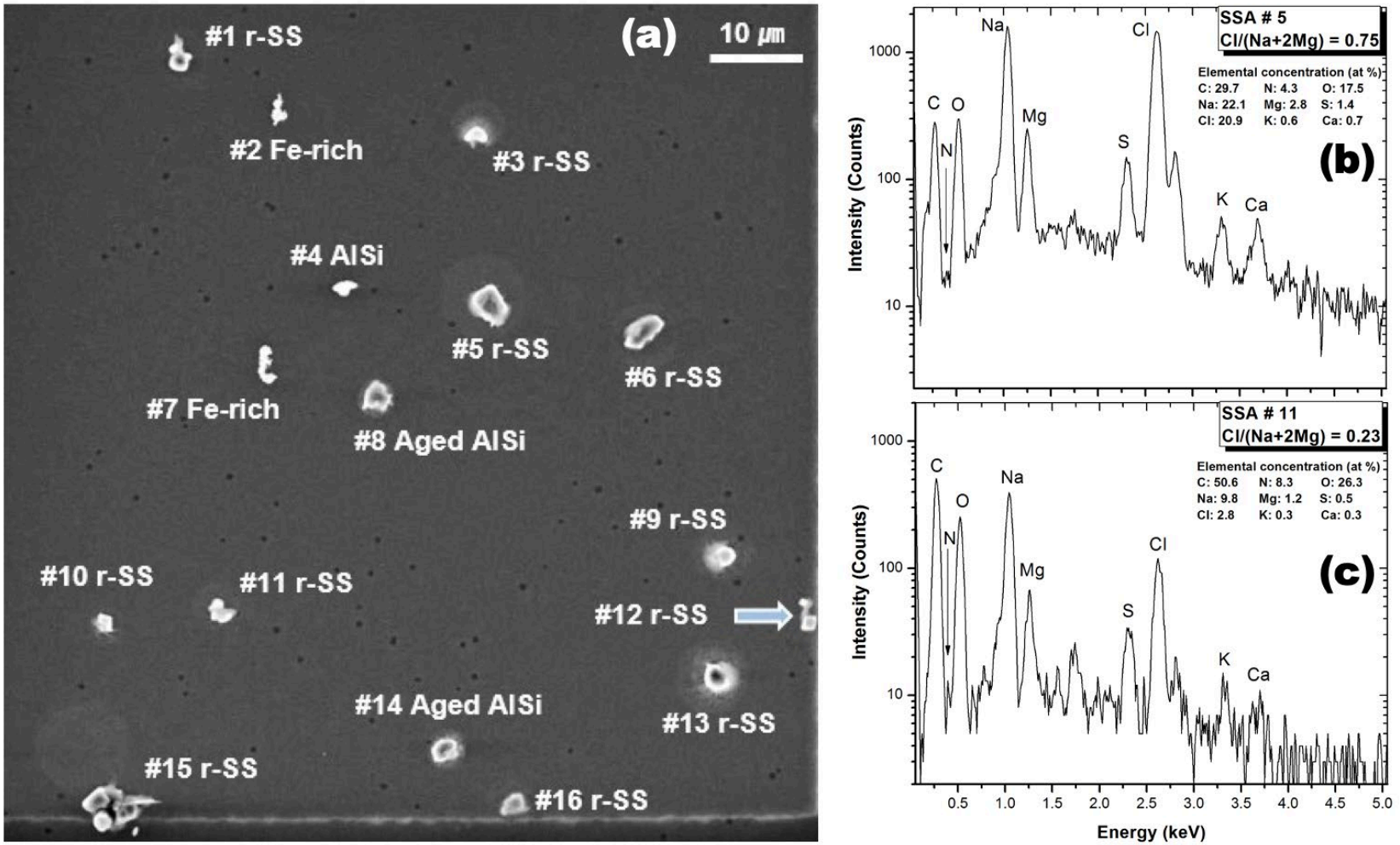

Figure 3. Optical images of the first field on TEM grid during humidifying (A-F, ↑) and dehydration (G-K, ↓) processes and the SEI of the same field (L).

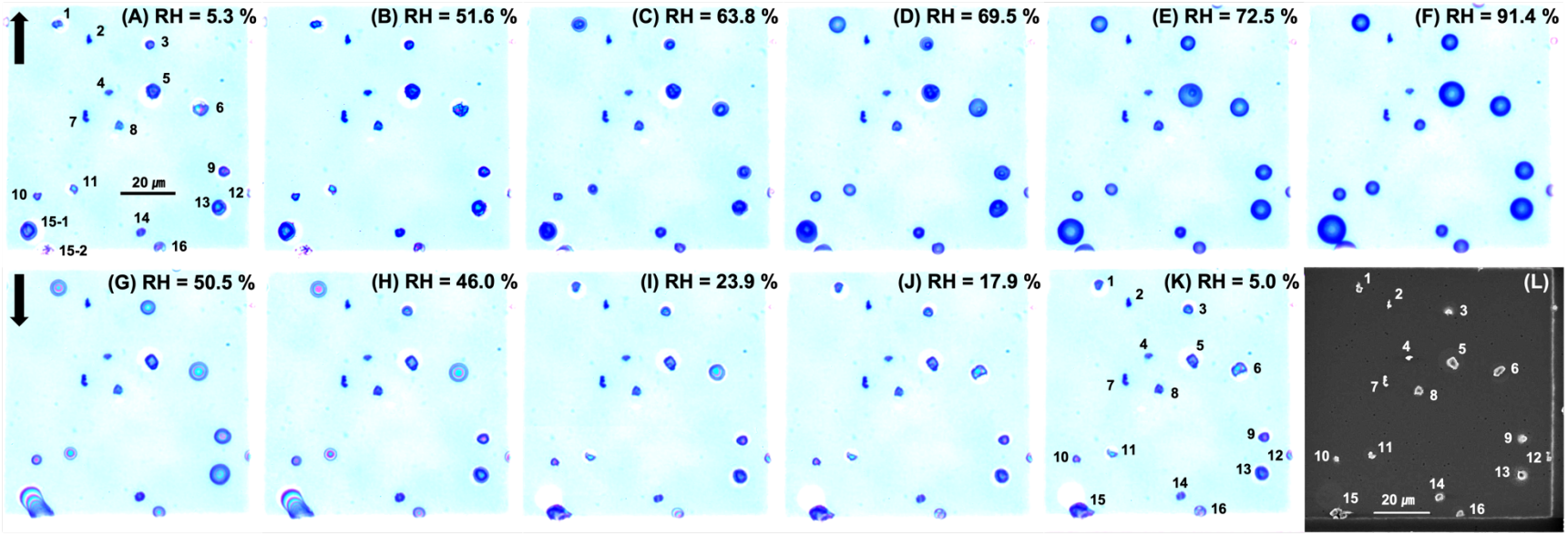

Figure 4. 2-D area ratio plot and optical images of Cl-rich SSAs #5 and #19 (a and d), 2-D area ratio plots of humidification (b and e) and dehydration (c and f) for the SSAs and (Na,Mg)(Cl,NO_3) particle as a function of RH.

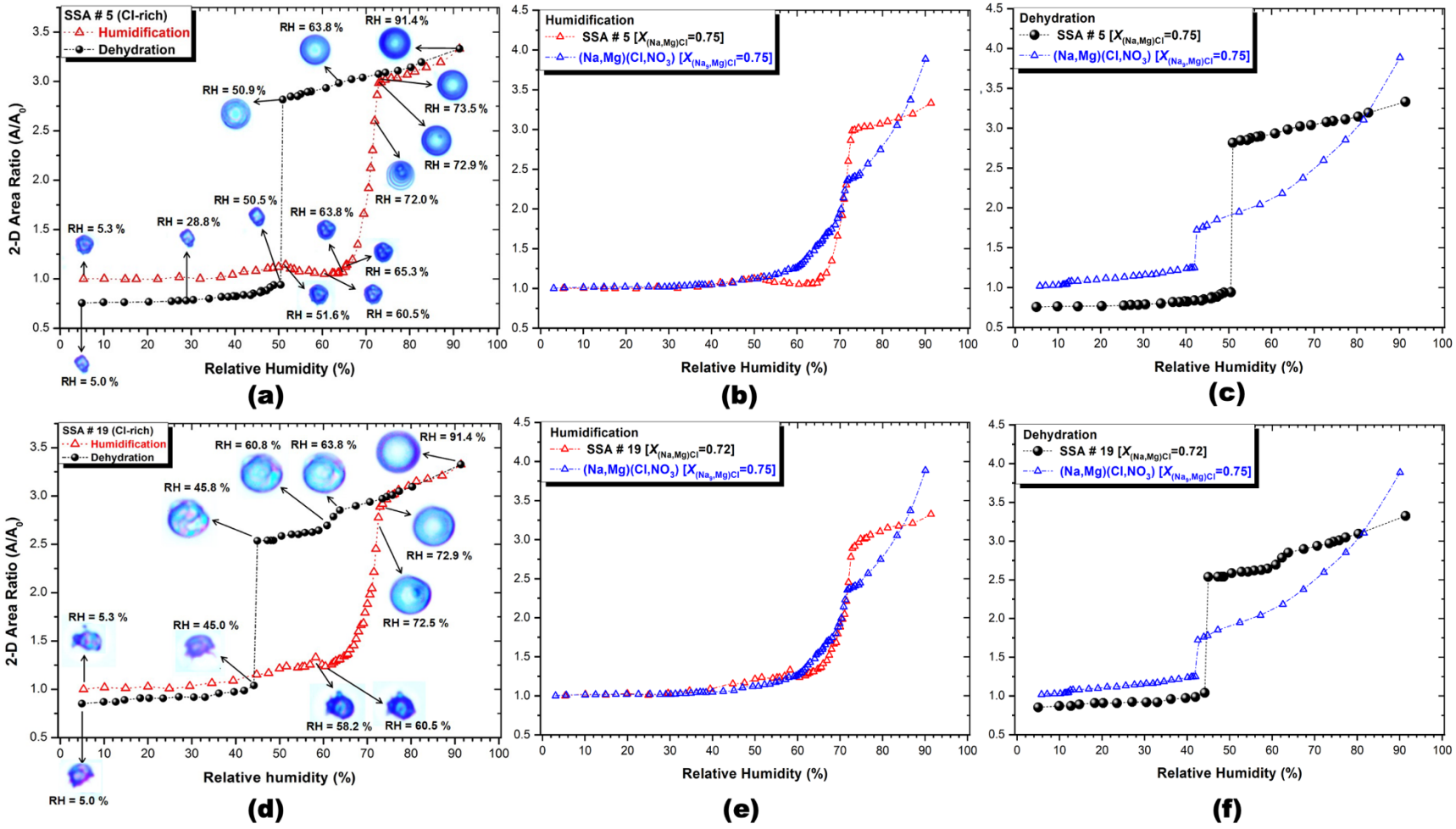

Figure 5. 2-D area ratio plot and optical images of an equimolar SSA #23 and a Cl-depleted SSA #11 (a and d), 2-D area ratio plots of humidification (b and e) and dehydration (c and f) for the SSAs and (Na,Mg)(Cl,NO_3) particles as a function of RH.

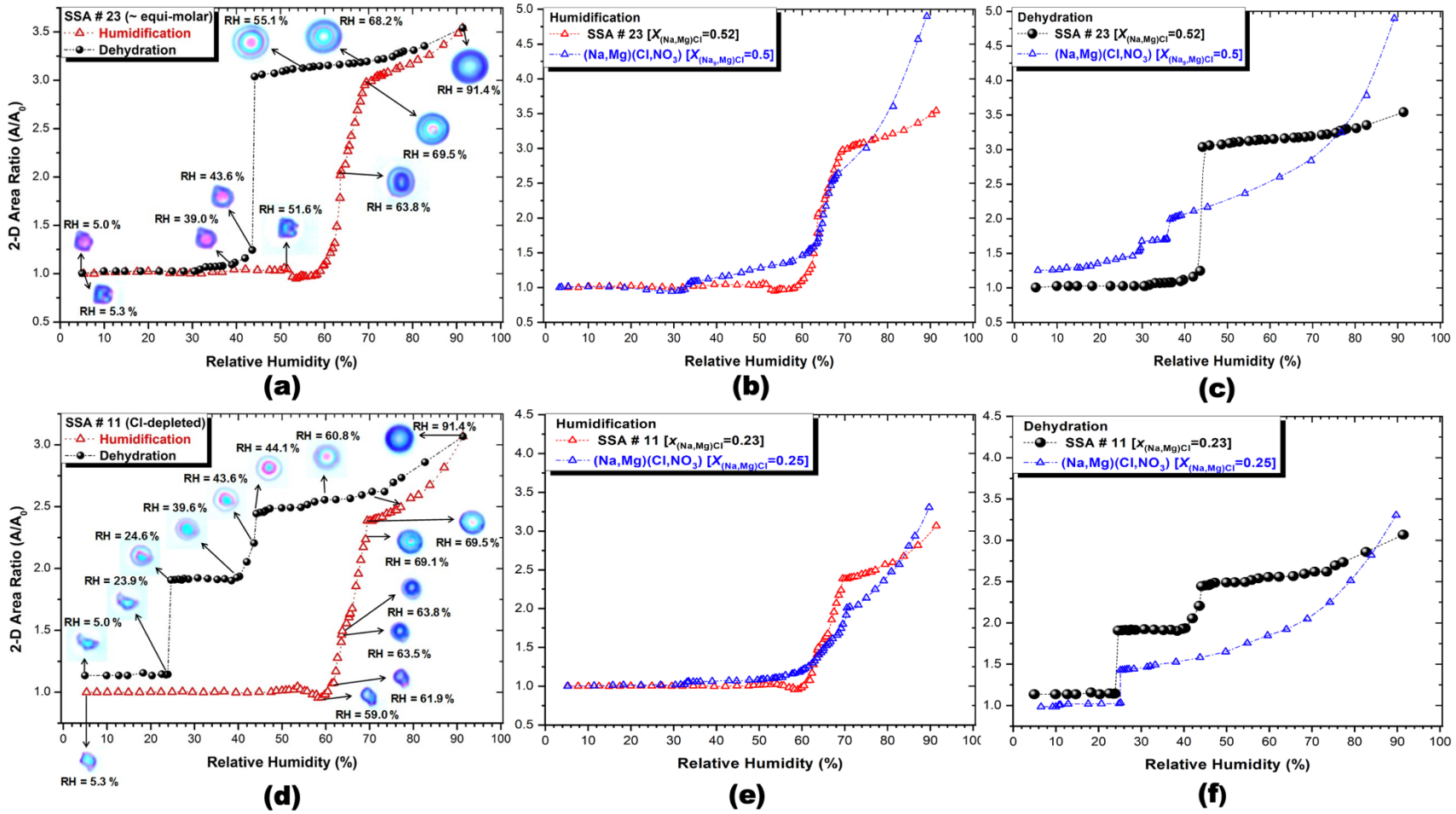

964 **Figure 6.** DRHs of ambient SSAs and (Na, Mg)(Cl, NO_3) and Na(Cl, NO_3) systems calculated from AIOMFAC plotted against the mole
965 fraction of chloride [$X_{(Na,\ Mg)Cl}$ or X_{NaCl}]. Major chemical components in each phase: P - all in solid phase; Q - aqueous eutonic
966 components + NaCl and (Na, Mg, Ca)(NO_3, SO_4, organics) in solid phase; R - $NaNO_3$ and (Ca, Na)SO_4 in solid phase + aqueous eutonic
967 components; S - NaCl and (Ca, Na)SO_4 in solid phase + aqueous eutonic components; T - aqueous phase for most components; black
968 vertical line – a eutonic composition of Na(Cl ,NO_3) system; blue vertical line – a eutonic composition of (Na, Mg)(Cl, NO_3) system.

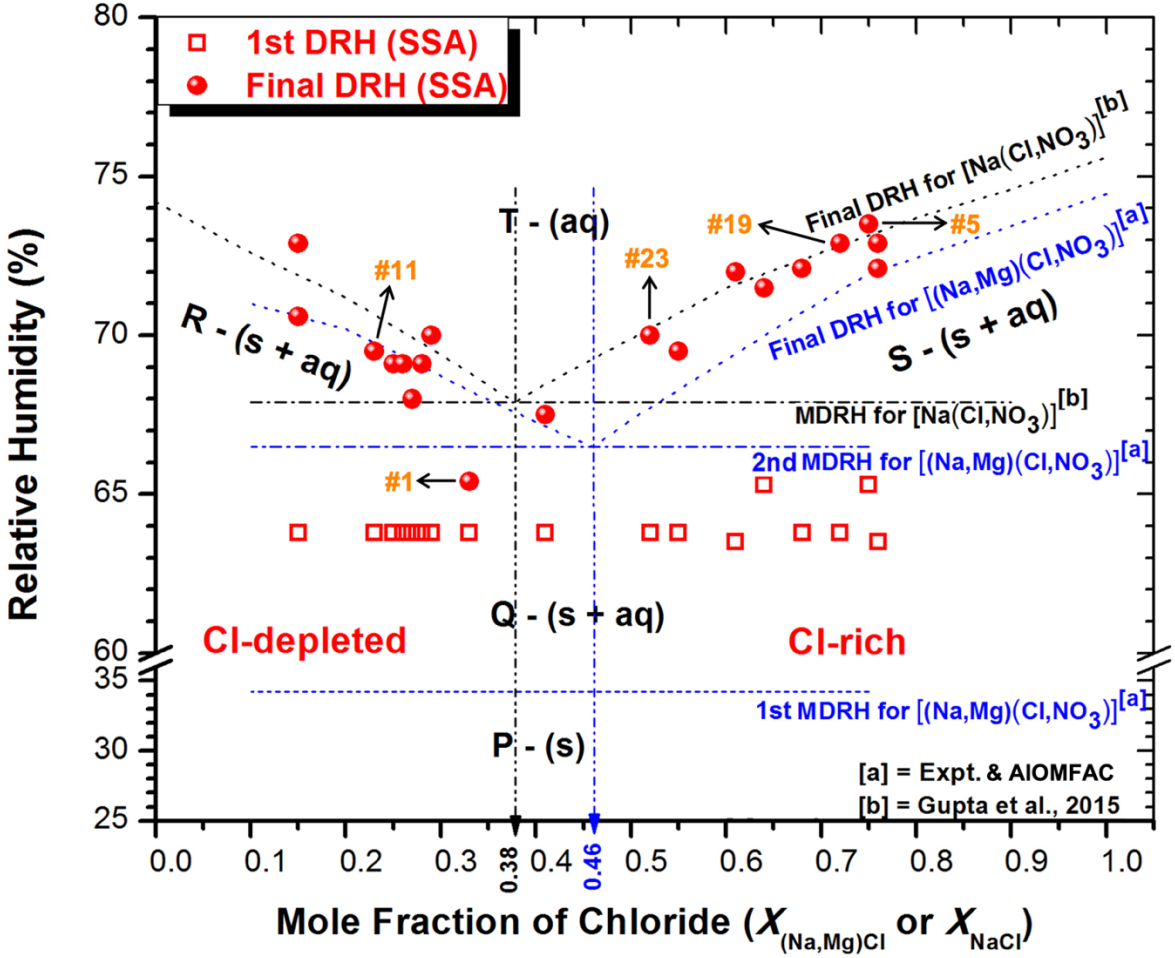

969

970 **Figure 7.** ERHs of ambient SSAs and those experimentally determined for (Na, Mg)(Cl, NO_3) and Na(Cl, NO_3) systems plotted against
971 the mole fraction of chloride [$X_{(Na,Mg)Cl}$ or X_{NaCl}]. Major chemical components in each phase: P –almost all components in aqueous phase;
972 Q - NaCl and other heterogeneously crystallized moieties in solid phase + aqueous nucleating species like $(Mg{\cdot}xH_2O)^{2+}$ and Cl^-/NO_3^-
973 $/SO_4^{2-}$; R - heterogeneously crystallized (Na, Mg)$NO_3{\cdot}xH_2O$ on crystalline (Ca, Na)$SO_4(xH_2O)$ seeds + aqueous NaCl and other
974 moieties; S - solid (Na, Mg, Ca)$(NO_3, SO_4){\cdot}xH_2O$ and homogeneously crystallized NaCl + aqueous/amorphous $(Mg{\cdot}xH_2O)^{2+}$ and NO_3^-
975 $/SO_4^{2-}$, and other minor species; T - all in solid phase; black vertical line - a eutonic composition of Na(Cl ,NO_3) system; blue vertical
976 line - a eutonic composition of (Na, Mg)(Cl, NO_3) system.

977

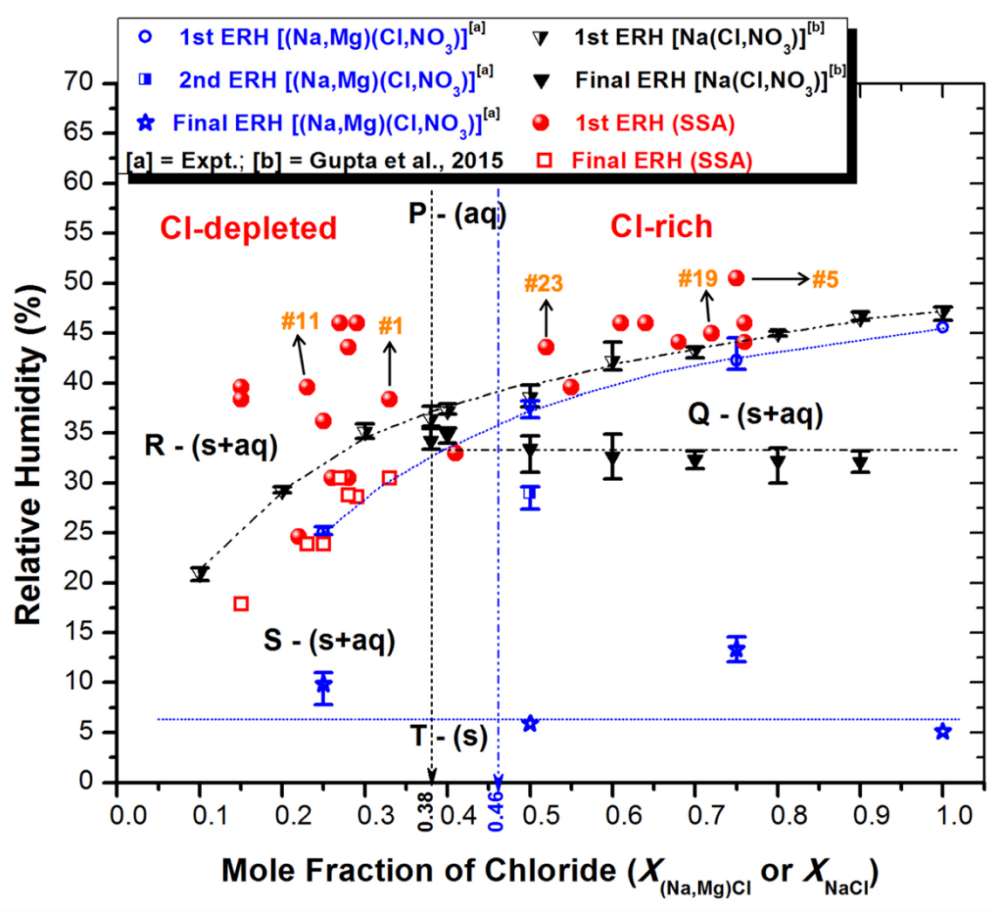

978

Figure 8. 2-D area ratio plot, X-ray spectrum, and SEM image with diameter of an aged aluminosilicate particle mixed with SSA (particle #14)